

Precursor Activity Preceding Interacting Supernovae – I: Bridging the Gap with SN 2022mop

S. J. Brennan^{*,1}, S. Barmantloo¹, S. Schulze², K. W. Smith^{3,4}, R. Hirai^{5,6,7}, J. J. Eldridge⁸,
 M. Fraser⁹, H. F. Stevance³, S. J. Smartt^{3,4}, S. Anand¹⁰, A. Aryan¹¹, T.-W. Chen¹¹, K. K.
 Das¹⁰, A. J. Drake¹², C. Fransson¹, A. Gangopadhyay¹, A. Gkini¹, W. V. Jacobson-Galán^{**,10},
 A. Jerkstrand¹, J. Johansson¹³, M. Nicholl¹⁴, G. Pignata¹⁵, N. Sarin^{1,16}, A. Singh¹, J.
 Sollerman¹, S. Srivastav³, B.F.A. van Baal¹, K. C. Chambers¹⁷, M. W. Coughlin¹⁸, H. Gao¹⁷,
 M. J. Graham¹⁰, M. E. Huber¹⁷, C.-C. Lin¹⁷, T. B. Lowe¹⁹, E. A. Magnier¹⁷, F. J. Masci²⁰, J.
 Purdum¹², A. Rest^{21,22}, B. Rusholme²⁰, R. Smith¹², I. A. Smith²³, J. W. Twedde³, R.J.
 Wainscoat¹⁷, and T. de Boer¹⁷

(Affiliations can be found after the references)

March 28, 2025

ABSTRACT

Over the past two decades, an increasing number of transients have exhibited luminous activity at their explosion sites weeks to years before an interacting supernova (SN) is observed. For some objects, this pre-SN activity is typically linked to large-scale mass-loss events preceding core collapse, yet its triggering mechanism and the underlying explosion process remain uncertain. We present SN 2022mop, which was initially observed in August 2022 exhibiting nebular emission, including [O I], Mg I, and [Ca II], resembling the late-time ($\gtrsim 200$ days post-explosion) spectrum of a stripped-envelope SN (SESN) from a progenitor with $M_{\text{ZAMS}} \lesssim 18 M_{\odot}$. SN 2022mop shows strong (~ 1 mag) repeating undulations in its light curve, suggesting late-time interaction. In mid-2024, the transient re-brightened for several months before a Type IIn SN ($r_{\text{peak}} = -18.2$ mag) was observed in December 2024, closely resembling the evolution of SN 2009ip. By triangulating both transients using Pan-STARRS images, we determine that both transients are coincident within ~ 3 pc. Given the environment, the chance alignment of two isolated SNe is unlikely. We propose a merger-burst scenario – a compact object formed in 2022, is kicked into an eccentric orbit, interacts with its hydrogen-rich companion over subsequent months, and ultimately merges with its companion, triggering a Type IIn SN-like transient.

Key words. supernovae: individual (SN 2022mop) – stars: mass loss – stars: circumstellar matter – stars: neutron

1. Introduction

The liberation of material from the stellar surface plays a crucial role in the life cycle and eventual demise of massive stars ($>8\text{--}10 M_{\odot}$; Chiosi & Maeder 1986; Smith 2014; Puls et al. 2008; Meynet et al. 2015; Leung et al. 2021; Laplace et al. 2021). The effects of mass loss are typically observed during the final SN explosions, where the progenitor’s chemical composition becomes apparent in the first few days to weeks following core-collapse (Niemela et al. 1985; Smartt 2009; Gal-Yam et al. 2014; Yaron et al. 2017; Gal-Yam 2017). Massive stars continuously eject material from their surface via stellar winds (Vink 2024) spanning several orders of magnitude ($\sim 10^{-8} - 10^{-4} M_{\odot} \text{ yr}^{-1}$), depending on their characteristics (e.g. mass, metallicity, and rotation). However, this may not be sufficient to account for the large amounts of confined material (as much as $0.1 M_{\odot}$ within 10^{15} cm; Tsuna et al. 2023; Ransome & Villar 2024) inferred from observations. The majority of massive stars are found in multi-stellar systems (Sana et al. 2012; Offner et al. 2023; Marchant & Bodensteiner 2024) and will likely interact with a companion star (Zapartas et al. 2017). Mass transfer can occur, removing large amounts of material via Roche-lobe overflow (RLOF; de Mink et al. 2013; Eldridge et al. 2017). The effect of binaries drastically alters the pre-SN progenitor, the amount of ejected circum-

stellar material (CSM), and the environment in which it explodes (Laplace et al. 2021), complicating our understanding of their evolution and interaction.

In this work we present SN 2022mop, which initially resembled a hydrogen-poor SESN during its nebular phase in August 2022. In late 2024, a transient at the position of SN 2022mop began to slowly re-brightened over several months, before an SN-like light curve was observed, with spectral observations indicating a hydrogen-rich interacting Type IIn SN classification. Section 2 outlines the discovery of SN 2022mop in 2022, its properties, as well as the photometric and spectroscopic observations. In Section 3, we investigate the alignment of the two events, as well as the environment in which the transient(s) occurred. Section 4 provides potential explanations for SN 2022mop, including the possibility of two separate SN explosions, as well as the second SN-like event being triggered by the merging of a hydrogen-rich star and a newly formed compact object.

2. Discovery and Follow-up Observations

2.1. SN 2022mop and Host Galaxy

SN 2022mop¹ was discovered by the Pan-STARRS collaboration on 12 June 2022 (Chambers et al. 2022), at a

¹ Also classified as ATLAS24saw, Gaia25aaf, GOTO25gj, PS22fhf, and ZTF22aanyxmg.

* Email: sean.brennan@astro.su.se

** NASA Hubble Fellow

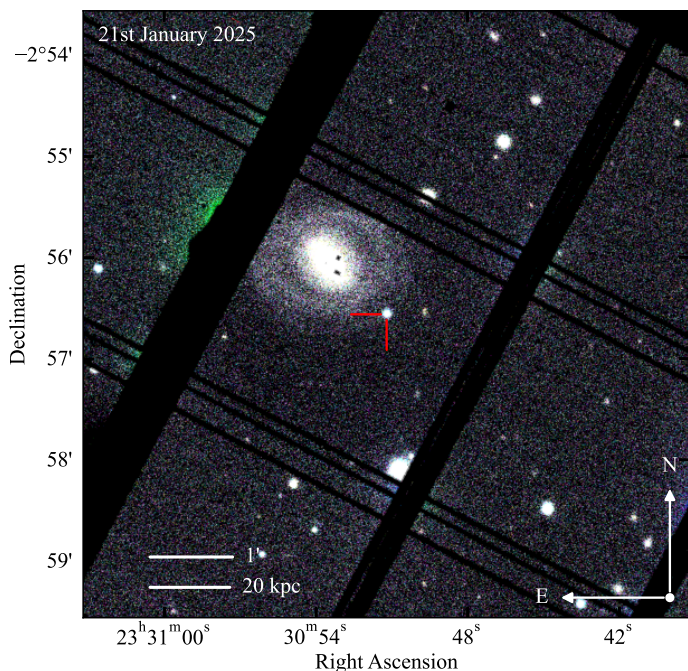


Fig. 1: Image of SN 2022mop and IC 1496, composed of 30s Pan-STARRS *gri* exposures taken near the peak of the 2024 transient. SN 2022mop, marked with red crosshairs, lies in a region of diffuse star formation approximately 16 kpc from the core of IC 1496, located at a luminosity distance of 70.7 Mpc. The diagonal black gaps represent chip gaps on the Pan-STARRS/GPC1 CCD detector.

magnitude of $w \sim 20.45$ mag. The location of the transient is approximately $46''$ from the core of the lenticular galaxy, IC 1496, as shown in Fig. 1. With a redshift of $z = 0.0169$ (Jones et al. 2004, 2009), this corresponds to a luminosity distance of 70.7 Mpc (distance modulus of 34.24 mag) and a separation of 16 kpc between SN 2022mop and the centre of IC 1496². We apply a correction for foreground Milky Way (MW) extinction using $R_V = 3.1$ and $E(B - V)_{MW} = 0.048$ mag (Schlafly & Finkbeiner 2011), with the extinction law given by Cardelli et al. (1989). No correction is made for any host extinction, as SN 2022mop is located in an isolated region and is unlikely to experience significant dust attenuation, as well as no strong evidence for Na I D absorption (Poznanski et al. 2012).

2.2. The 2024 Rebrightening of SN 2022mop

For clarity and consistency with similar objects (e.g. SN 2009ip; Smith et al. 2008; Foley et al. 2011; Pastorello et al. 2013; Margutti et al. 2014), we refer to the entire evolution of the transient as SN 2022mop, distinguishing between the 2022 and 2024 transients accordingly. SN 2022mop re-emerged in August 2024 and was identified (priv. comm.) as a late-time rebrightening of an SESNe (e.g. Chen et al. 2018; Sollerman et al. 2020). On the 28th December 2024, SN 2022mop exhibited a sharp increase in brightness (Srivastav et al. 2025), with a light curve evolution now resembling the pre-SN activity seen in hydrogen-rich Type II_n/Ib_n SNe shortly before

² We assume a Hubble constant $H_0 = 73 \text{ km s}^{-1} \text{ Mpc}^{-1}$, $\Omega_\Lambda = 0.73$, and $\Omega_M = 0.27$ (Spergel et al. 2007).

core collapse (Pastorello et al. 2013; Strotjohann et al. 2021; Brennan et al. 2024b). The 2024 transient peaked in the *r*-band on 13 January 2025 (MJD: 60688.39) with a peak apparent magnitude of $r = 16.40 \pm 0.02$ mag, with spectral observations showing strong emission from the Balmer series (Sollerman et al. 2025).

2.3. Photometric Observations and Evolution

Science-ready images obtained as part of the ZTF survey (Bellm et al. 2019; Graham et al. 2019; Dekany et al. 2020; Masci et al. 2019) were acquired in *gri* from the NASA/IPAC Infrared Science Archive (IPAC³) service. Template-subtracted photometry was performed using the AutoPhOT pipeline (Brennan & Fraser 2022); see Appendix A for further details. No significant activity or outbursts were detected in pre-discovery images extending back to the beginning of ZTF observations (circa-2018), with a limiting absolute magnitude of approximately -14 mag. Photometry from the ATLAS forced-photometry server⁴ (Tonry et al. 2018; Smith et al. 2020; Shingles et al. 2021) was obtained in the *c* and *o* bands. We computed the weighted average of the fluxes of observations on a nightly cadence. A quality cut at 5σ was applied to the resulting nightly fluxes for both filters, after which the measurements were converted to the AB magnitude system.

The field of SN 2022mop was observed as part of regular Pan-STARRS (Chambers et al. 2016) operations in 2022 in *w* and *i* filters. Following the 2024 rebrightening, we obtained targeted follow-up observations with PS in the *grizy* filters. The PS data were processed with the Image Processing Pipeline (Magnier et al. 2020a; Waters et al. 2020; Magnier et al. 2020b,c). We also utilised the 40 cm SLT telescope at the Lulin observatory and obtained images in SDSS *ugriz* filters as part of the Kinder collaboration (Chen et al. 2024b). Images were calibrated using a custom built pipeline⁵ and photometrered using the AutoPhOT pipeline. We retrieve Dark Energy Camera (DECam) images covering the site of SN 2022mop from the NOIR-LAB data archive⁶, including data from 2022⁷ (#2020B-0053, PI. Brout). No activity is detected prior to 2022. SN 2022mop is visible in unfiltered images (calibrated to the *r*-band) from the Catalina Sky Survey's (Drake et al. 2009) 1.5m Mount Lemmon Survey (MLS) telescope, taken on 27th May 2022, and was observed again on 12th September 2024. No clear prior prior to 2022 is seen in additional MLS observations dating back to September 2010. Additionally, we photometer unfiltered images from Spacewatch (McMillan et al. 2015), also calibrated to the *r*-band, taken sporadically from 2003 to 2015. No significant activity is detected.

The field of SN 2022mop was observed with the Wide-field Infrared Survey Explorer (WISE) instrument in the W1 and W2 bands during the NEOWISE-reactivation mission (NEOWISE-R; Mainzer et al. 2014). Single exposures in the W1 and W2 bands were collected from the NASA/IPAC Infrared Science Archive (IRSA) and coadded using the ICORE service (Masci 2013). Reference im-

³ <https://irsa.ipac.caltech.edu/applications/ztf/>

⁴ <https://fallingstar-data.com/forcedphot/>

⁵ <https://hdl.handle.net/11296/98q6x4>

⁶ <https://datalab.noirlab.edu/sia.php>

⁷ <https://astroarchive.noirlab.edu/portal/search/>

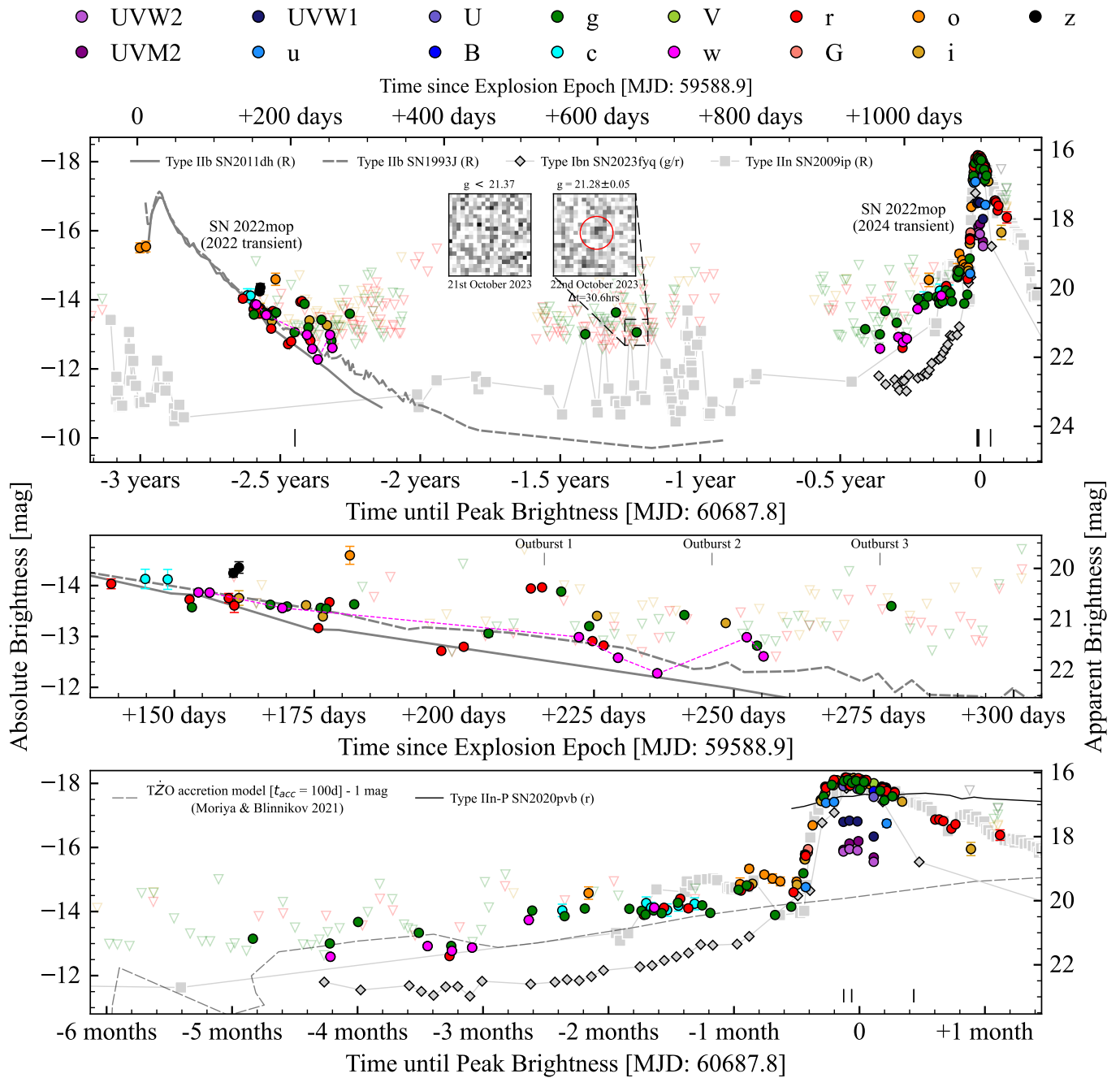


Fig. 2: *Upper Panel*: Optical light curve evolution of SN 2022mop over ~ 3 years since discovery, covering both the 2022 and 2024 transients. Vertical black lines indicate when spectra were obtained. *Middle panel*: The 2022 event resembles a hydrogen-poor SN (see Section 3.2) but exhibits a bumpy decay seen in Pan-STARRS and ZTF photometry, that is inconsistent with purely ^{56}Ni -powered emission. These outburst or flares likely require additional energy input from CSM interaction. *Lower panel*: The 2024 event resembles an interacting hydrogen-rich transient, such as SN 2009ip, with a ~ 4 -month-long pre-SN rise, followed by a transient that photometrically and spectroscopically resembles an interacting SN.

ages were created by coadding data from 2015, which were subtracted from the subsequent images.

UV photometry was obtained using the Ultra-Violet Optical Telescope (UVOT) onboard the *Neil Gehrels Swift Observatory* (Gehrels et al. 2004; Roming et al. 2005). Image reduction was performed on non-template subtracted

images using the *Swift* HEASoft package⁸. A log of photometric observations is provided in Table A.1 and illustrated in Fig. 2.

Our photometric coverage of the 2022 transient is limited due to the field being in solar conjunction when the transient was expected to reach peak brightness. Two AT-

⁸ <https://heasarc.gsfc.nasa.gov/docs/software/heasoft/>

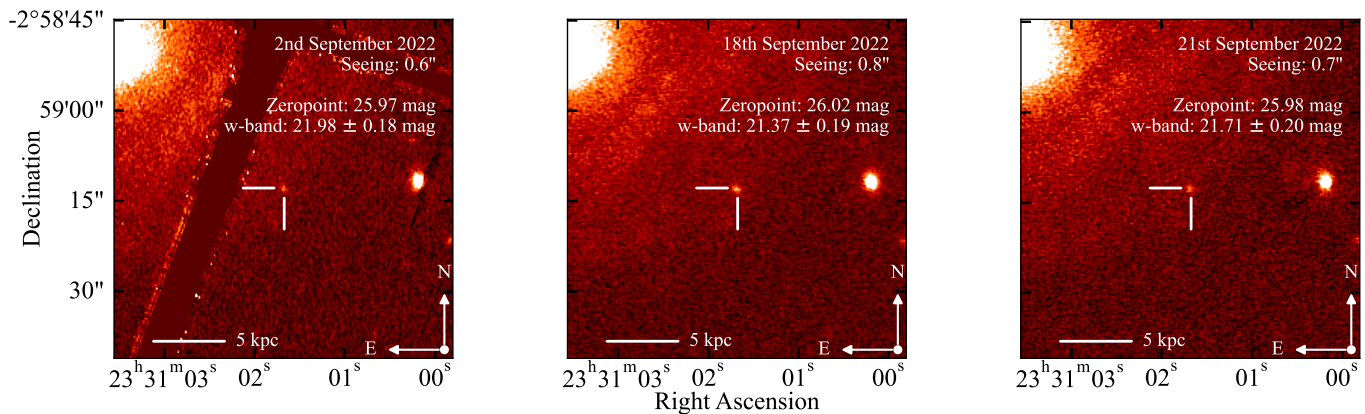


Fig. 3: Pan-STARRS w -band cutouts of SN 2022mop from September 2022 during the transient’s nebular phase. Over approximately three weeks, the transient brightened by ~ 0.6 magnitudes before fading, see Fig. 2. This rebrightening may indicate late-time CSM interaction. See Section 4.2 for further discussion.

LAS observations (both $S/N > 5$) in the o -band capture the initial rise of SN 2022mop. Following its return from solar conjunction, photometry from Pan-STARRS, ATLAS, and ZTF captures the nebular phase decline until the transient fades beyond detection limits.

SN 2022mop exhibits outburst-like events from ~ 215 days post-explosion (see Appendix B for the explosion time (t_{exp}) estimation). During its smooth decline, a > 1 mag outburst occurs in all bands. Neighbouring non-detections constrain this rise to at least 1.5 mag in ~ 3 days, followed by a ~ 20 -day decline. Around 250 days post-explosion, a ~ 0.6 mag bump is observed (Fig. 3), primarily in the w -band from Pan-STARRS, with sporadic detections in ZTF g and r . A potential third outburst is observed around ~ 275 days post-explosion, although the cadence around this epoch is low. These outbursts may be repeating, with a period of approximately 27 days (about twice as long as that reported for SN 2022jli; Moore et al. 2023; Chen et al. 2024a), as well as decreasing magnitude. To investigate further, we bin available ZTF gri images during this phase. As shown in Fig. 4, there is a resemblance between these outburst and the initial appearance of SN 2009ip in 2009, overall resembling a sawtooth like lightcurve with the peaks separated by ~ 30 days, potentially suggesting a similar powering mechanism. It should be noted that spectra of SN 2009ip around this time show strong signs of interaction with H-rich material (Smith et al. 2010; Foley et al. 2011; Pastorello et al. 2013), unlike what is observed for SN 2022mop. Further efforts are required to rigorously account for this flaring, which is beyond the immediate goals of this work.

SN 2022mop was detected again around 1.5 years post-explosion in the g -band that again, must be occurring on rapid timescales (i.e. a few a days), as indicated by neighbouring non-detections. This behaviour is reminiscent of the 2010 – 2011 eruptions from the progenitor of SN 2009ip (Pastorello et al. 2013), reaching similar magnitudes and timescales. While our optical detections are this phase are limited, we also detect SN 2022mop in the mid-infrared, see Fig. A.1. The origin of this emission remains unclear, though it has been proposed that such pre-SN outbursts are driven by ejecta or outflow interaction with clumpy CSM

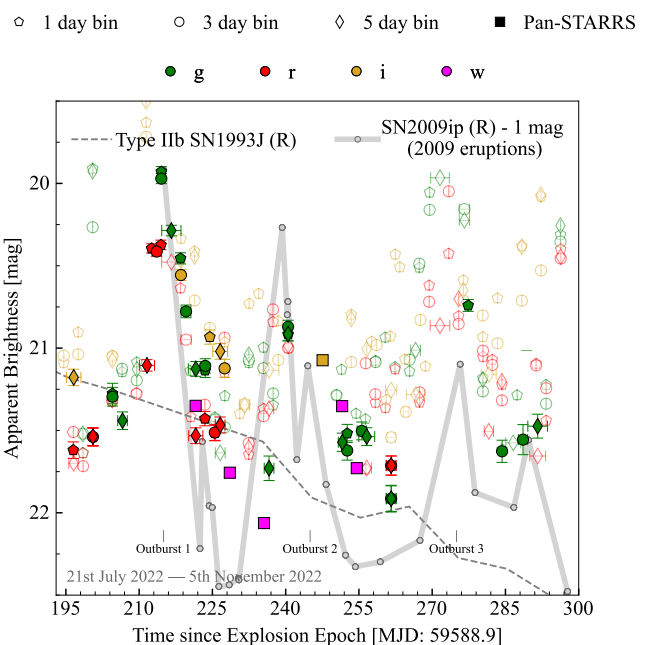


Fig. 4: Re-binned ZTF light curve of SN 2022mop during the 2022 decline. Images are stacked into their respective bins, given in the upper legend, and processed as described in Section 2.3. Filled markers denote points with $S/N > 3$, where the source meets detection criteria via artificial source injection. The 2022 decline phase exhibits several outbursts/flares, roughly 27 days apart, loosely resembling the 2009 eruptions of SN 2009ip (Pastorello et al. 2013) (solid grey line, fit by eye). The dashed line the the radioactive powered tail of SN 1993J, highlighting the strong divergence from a ^{56}Ni powered decline.

or by binary interaction (Soker & Kashi 2013; Kashi et al. 2013).

Following its 2024 solar conjunction, SN 2022mop was observed to brighten continuously⁹ from August 2024 over the subsequent four months, rising by approximately one magnitude in all bands. Although the detection cadence is suboptimal, the light curve shows some structure, beginning with a bump lasting about one month, followed by a more gradual rise. Similar to SN 2009ip’s Event A, which exhibited a decline of approximately one magnitude before the onset of Event B, SN 2022mop shows a similar trend, mainly seen in the g -band. Subsequently, SN 2022mop exhibits a SN-like rise on 28th December 2024, with a rise time of ~ 12 days, typical of Type II_n SNe (Taddia et al. 2013; Nyholm et al. 2020).

As the 2024 transient evolves post-peak, the field begins to set, limiting observations. Several epochs were obtained using ZTF and Lulin facilities around 20 days post-peak. A single ZTF r -band data point shows a small bump in the light curve at approximately 25 days post-peak. A similar bump was observed for SN 2009ip (e.g. Kashi et al. 2013) and is common in the post-peak evolution of several interacting transients (Nyholm et al. 2020).

2.4. Spectroscopic Observations and Appearance

SN 2022mop was observed on 1st August 2022 as part of the Census of the Local Universe (CLU) survey (Cook et al. 2019; De et al. 2020) using the Low Resolution Imaging Spectrometer (LRIS; Oke et al. 1995) on the 10-m Keck telescope; see Fig. 5. Prior to these observations, SN 2022mop was in solar conjunction meaning the peak lightcurve phase was missed. Due to strong emission from [O I], Mg I, and [Ca II], SN 2022mop resembled a typical nebular SESN and received minimal follow-up.

Motivated by the 2024 rebrightening in December 2024, follow-up spectra were obtained using the Nordic Optical Telescope (NOT) with the Alhambra Faint Object Spectrograph and Camera (ALFOSC) and Keck/LRIS. The spectra were reduced in a standard manner using PyPeIt (Prochaska et al. 2020a,b; Prochaska et al. 2020) and LPipe (Perley 2019) respectively, with observations coordinated using the FRITZ data platform (van der Walt et al. 2019; Coughlin et al. 2023). Further discussion of spectroscopic features is given in Section. 3.2 and 4.1. An observation log of spectral observations is given in Table. A.3 and illustrated in Fig. 5 and A.2.

3. Methods and Analysis

3.1. Coincidence Between the 2022 and 2024 Transients

We investigate the possibility that the 2022 and 2024 transient are two isolated events that coincidentally occupy the same pixel on the CCD detector (similar to the recent SN 2020acct; Angus et al. 2024). Using common sources in both images, we triangulate the position of the 2022 transient, projected on the 2024 image. To address sampling concerns (e.g. Nyquist criteria), we construct an oversampled PSF and fit for the transient’s position using a Monte

Carlo approach, see Appendix D for further discussion¹⁰. The results of this triangulation are shown in Figs. 6 and 7.

We report that both events coincide within 0.02 ± 0.25 pixels or 0.007 ± 0.062 arcseconds. Given the distance to IC 1496, this corresponds to 2.39 ± 21.23 parsecs. To refine this measurement, we conducted systematic tests, including *Jackknife* resampling¹¹. We measure a refined separation of 2.786 ± 0.761 parsecs. This analysis assumes that the Pan-STARRS/GCP1 CCD remained stable between epochs (we do not account for unexpected image flexure or defects beyond reprojecting each image to correct distortions) and the oversampled PSF adequately fits the source position.

3.2. Modelling the Progenitor of SN 2022mop with SUMO

To obtain further insights into the progenitor (system) that lead to SN 2022mop, we attempt to model the August 2022 Keck/LRIS spectrum of the first event using the SUPernova MOnTe carlo code (SUMO; Jerkstrand 2011; Jerkstrand et al. 2012, 2014). SUMO is a Monte Carlo radiative transfer code operating in non-local thermodynamic equilibrium (NLTE), which solves for the temperature, excitation, and ionisation structure of the ejecta, resulting in a model spectrum.

Due to the similarities with other SESNe nebular spectra, we use the helium star models from Woosley (2019); Ertl et al. (2020) as inputs for spectral modelling. These pre-SN models provide the chemical composition, mass and velocity for SN ejecta for a range of progenitor helium stars of $M_{\text{He, init}} \sim 3 - 12 M_{\odot}$. Based on comparison to earlier spectra for these models (Dessart et al. 2021, 2023; Barmantloo et al. 2024), we create model spectra for three of these progenitors, namely those with $M_{\text{He, init}} = 3.3, 4.0$ and $6.0 M_{\odot}$. The final model spectra are presented and compared to SN 2022mop in Figure 8. Further details on model setup are given in Appendix C.

The [O I] $\lambda\lambda 6300, 6364$ doublet, which is one of the primary diagnostics for progenitor mass (Jerkstrand et al. 2015), is best reproduced by the HE4P0 model. The strength of the [N II] $\lambda\lambda 6548, 6583$ is another diagnostic of progenitor mass (Barmantloo et al. 2024), that may be used for spectra with epochs $\gtrsim 200$ d. As our estimated epoch for the August 2022 SN 2022mop spectrum is 206 ± 6 d post explosion, we determine the $f_{[\text{N II}]}$ value as described in Barmantloo et al. (2024) and find $f_{[\text{N II}]} = 6.1$, which is equal to the value found for their HE4P0 model (i.e. $M_{\text{He, init}} = 4.0 M_{\odot}$) at an epoch of 200 d. Another feature of interest in the SN 2022mop spectrum is found around 5700 \AA . We identify this feature as [N II] $\lambda 5754$ (Jerkstrand et al. 2015; Dessart et al. 2021; Barmantloo et al. 2024). Comparing to the sample study in Barmantloo et al. (2024), [N II] $\lambda 5754$ is stronger in SN 2022mop than in typical SESNe. Analogously to the [O I] $\lambda 5577$ /[O I] $\lambda\lambda 6300, 6364$ pair, [N II] $\lambda 5754$ is a transition from the 2nd to the 1st excited state, whereas [N II] $\lambda\lambda 6548, 6583$ is from the 1st ex-

¹⁰ The open source code to perform these alignments can be found at <https://github.com/AstroSean/TransientTriangulator>.

¹¹ *Jackknife* resampling systematically omits one observation at a time from a dataset, recalculates the statistic of interest for each subset, and aggregates the results to estimate bias and variance (Cochran 1946).

⁹ SN 2022mop may be experiencing flickering events during this rise, but due to the low cadence observations this is difficult to falsify.

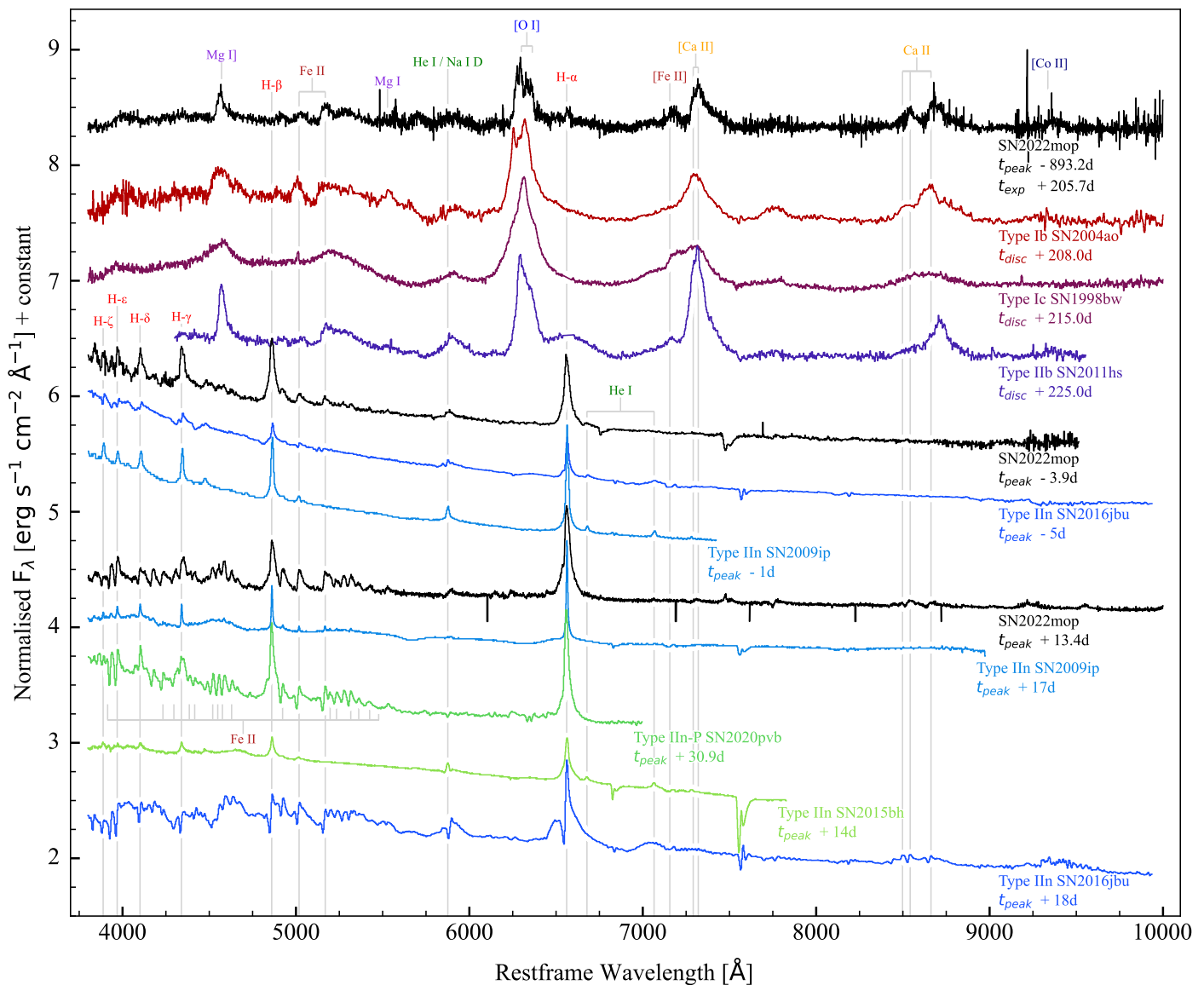


Fig. 5: Spectral comparison of SN 2022mop with other relevant SNe. All spectra have been corrected for redshift and MW extinction. SN 2022mop was observed in August 2022 and resembled a SESN during the nebular phase, e.g. SNe 2004ao (Modjaz et al. 2014), 1998bw (Patat et al. 2001), and 2011hs (Bufano et al. 2014). Over two years later, SN 2022mop experienced a dramatic rebrightening, resembling a hydrogen-rich interacting transient similar to SN 2009ip (Pastorello et al. 2013; Fraser et al. 2013) and SN 2015bh (Elias-Rosa et al. 2016; Thöne et al. 2017). Post-peak spectral observations closely match those of interacting transients that show pre-SN activity including SN 2016jbu (Kilpatrick et al. 2018; Brennan et al. 2022), and classified Type IIc-P SNe (SN 2020pvb; Elias-Rosa et al. 2024).

cited state to the ground state. The presence of [N II] $\lambda 5754$ in the observed spectrum is thus indicative of a relatively high temperature ($T_e \approx 10^4$ K within the He/N zone) or density, confirming that it must indeed be an early ($\lesssim 200$ d) nebular spectrum. Furthermore, it confirms the presence of a He/N envelope in SN 2022mop, removing the possibility of SN 2022mop being a Type Ic event (Barmantloo et al. 2024).

The nebular modelling points to SN 2022mop originating from a star with $M_{\text{He, init}} \sim 4.0 M_{\odot}$. Following the stellar modelling by Woosley (2019); Ertl et al. (2020), such a progenitor would lead to $M_{\text{ej}} \sim 1.6 M_{\odot}$ of hydrogen-poor ejecta. Assuming that the hydrogen envelope was stripped through binary transfer at the start of central helium burning, this translates to $M_{\text{ZAMS}} \sim 18 M_{\odot}$ (i.e.

following the evolution given in Woosley 2019; Ertl et al. 2020). In case the hydrogen envelope was lost later, the extended growth of the He-core through hydrogen shell-burning would require a lower M_{ZAMS} to produce the same mass of hydrogen-poor ejecta and $M_{\text{He, init}}$ mass, meaning we set a limit to the progenitor's $M_{\text{ZAMS}} \lesssim 18 M_{\odot}$.

One feature that our models clearly overestimate is the red side of the Ca NIR triplet around 8700 Å, likely caused by strong [C II] $\lambda 8727$ emission. Understanding why this is overproduced is outside of the scope of this work, but will be discussed in a future paper (S. Barmantloo. et al. 2025 in prep). Due to limitations of the SUMO code, our models do not account for asymmetries in the system. As shown in Fig. 9, the [O I] $\lambda\lambda 6300, 6364$ emission feature exhibits a double-

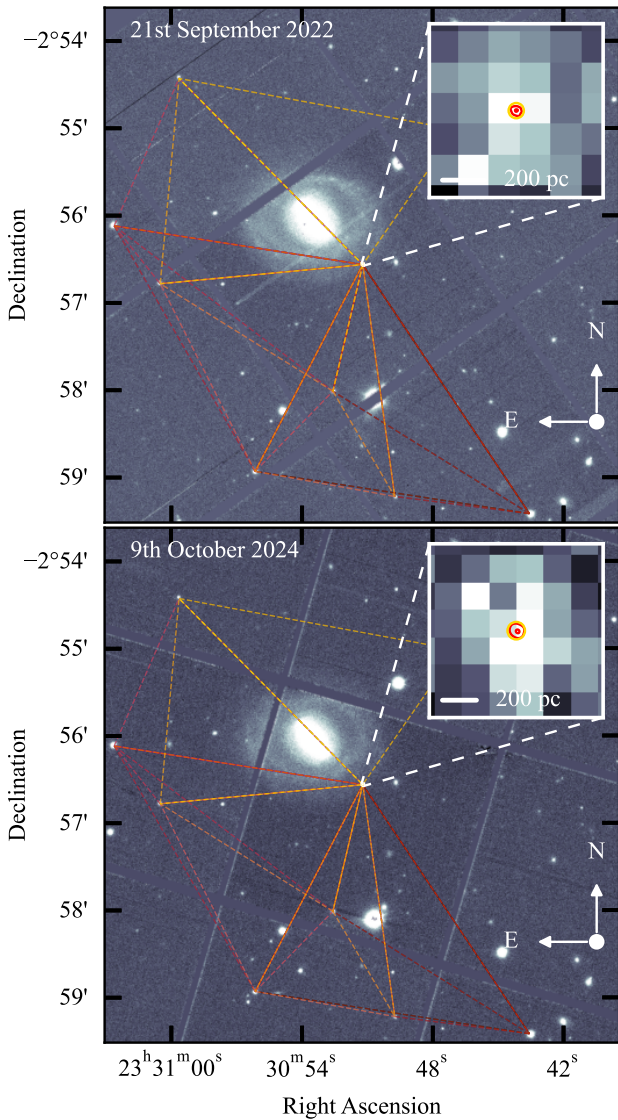


Fig. 6: Triangulation of the 2024 source based on the fitted position of the 2022 source using triangulation of matching sources both images. Positions were determined using a point-spread functions built using bright, isolated sources in each image. Each inset shows the fitted position (gold) and the triangulation contours (1 and 2 σ regions given in red) for each epoch.

peaked structure, with components blueshifted by 300 and 1100 km s⁻¹, respectively. This is a common feature in SESNe nebular spectra (Modjaz et al. 2008; Maeda et al. 2008; Taubenberger et al. 2009; van Baal et al. 2024) and is likely caused by ejecta expanding in a torus- or disk-like geometry.

3.3. Properties of SN 2022mop's Environment

There is significant emission at the position of H α in the August 2022 spectrum of SN 2022mop (see Fig. 10). The

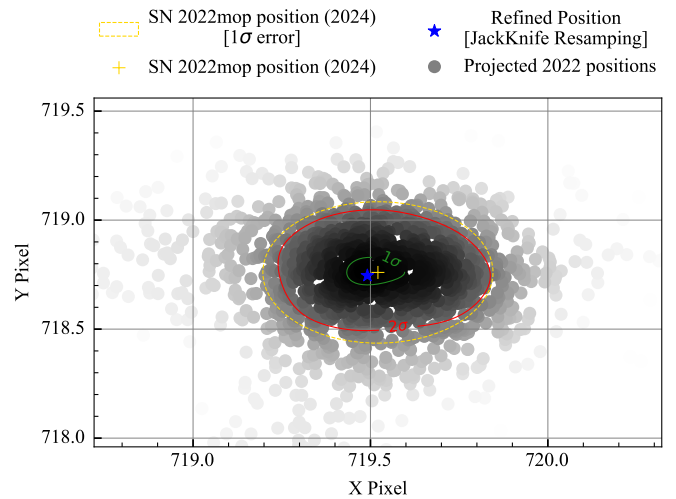


Fig. 7: The 2022 transient positions (black points) projected onto the 2024 image using `TransientTriangulator`. The gold region represents the 1 σ fitted position of the 2024 transient. The alignment of the 2022 and 2024 transients within their 1 σ uncertainties results in an offset of 0.020 ± 0.25 pixels or ~ 2.3 parsecs.

width¹² of this feature (~ 800 km s⁻¹) suggests that it originates from SN 2022mop, and any true host emission is likely to be fainter than this. However, we also consider the possibility that it may arise from the underlying host environment. We measure a line luminosity of $1.35 \pm 0.23 \times 10^{-16}$ erg s⁻¹ cm⁻². If this flux originates from the environment surrounding SN 2022mop, it would correspond to a star formation rate (SFR) of $\sim 10^{-4}$ M $_{\odot}$ yr⁻¹ using the relation from Kennicutt (1998). Assuming a flat continuum with an emission profile of similar luminosity, this would correspond to an apparent r -band magnitude of ~ 26 . At this brightness, it would not be detectable in Fig. 11, assuming a point-like cluster.

Assuming a Salpeter initial mass function (IMF) (Salpeter 1955) of the form $\xi(m) = \xi_0 \cdot m^{-2.35}$, we estimate the supernova rate (SNR) using the relation $\text{SNR} = \kappa \cdot \text{SFR}$ ¹³. The efficiency factor (κ) serves as a proportionality constant and is roughly given as $\kappa \approx \frac{0.01}{\text{M}_{\odot} \text{ yr}^{-1}}$ (Dahlén & Fransson 1999). Given an SFR of $\sim 10^{-4}$ M $_{\odot}$ yr⁻¹, the vicinity of SN 2022mop would be expected to produce ~ 1 SN/Myr.

While the scenario of two isolated transients occurring in the same local environment is disfavoured, it remains difficult to falsify. It is possible that two massive stars originated within the same cluster. Since stars in a cluster are generally assumed to be coeval (Soderblom 2010), these two progenitors must have undergone different evolutionary pathways (but have coordinated core-collapse), as motivated by their distinct chemical signatures. Although one

¹² This feature is resolved given the Keck/LRIS setup on 3rd August 2022, which used a 1'' slit, with seeing conditions of 1.09'', and the measured values are $\text{FWHM}_{\text{obs}} = 18.6 \text{ \AA}$, $\text{FWHM}_{\text{inst}} = 6.9 \text{ \AA}$, with a dispersion of 1.16 $\text{\AA}/\text{arcsec}$, yielding a minimum resolution of 320 km s⁻¹.

¹³ For the SFR_{MW} of $\sim 2 \text{ M}_{\odot} \text{ yr}^{-1}$ (Elia et al. 2022), this results in the common consensus of 1–2 Galactic SNe per century (Rozwadowska et al. 2021).

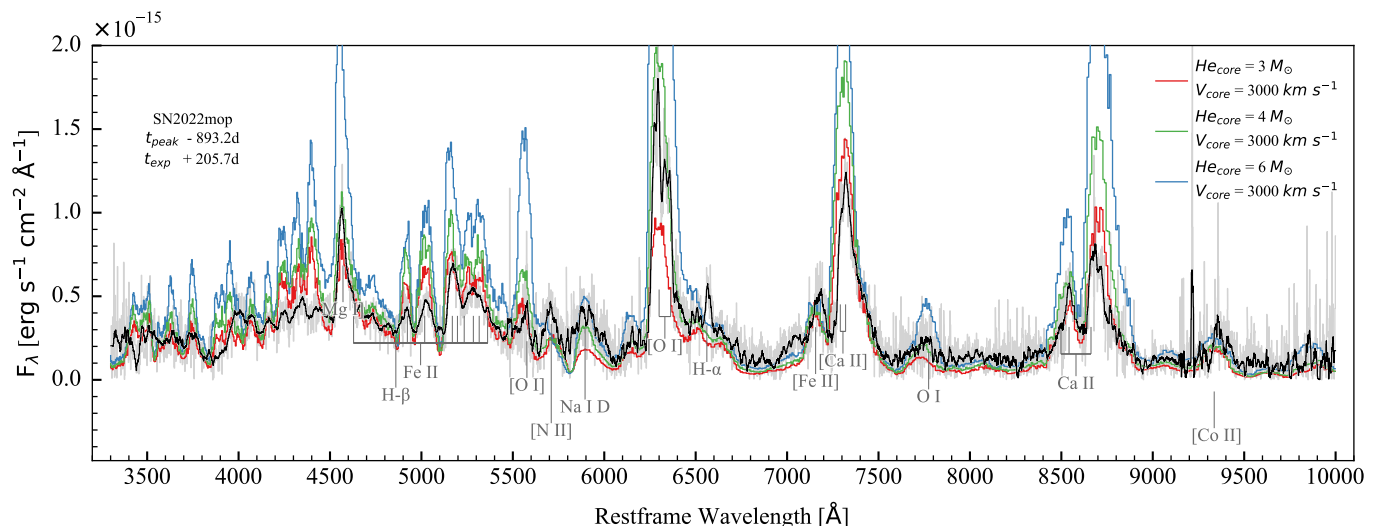


Fig. 8: A comparison between our SUMO model spectra and the Keck/LRIS spectrum of SN 2022mop from August 2022. For clarity, we smooth the observed spectrum (black line, with the original spectrum given in grey). The computed models and SN 2022mop spectrum have been scaled to a distance of 10 Mpc, and the models have been simulated with a ^{56}Ni mass of $0.06 M_{\odot}$ (which is consistent with SN 1993J, see Fig. 2). Line identifications of the most prominent emission lines have been added. The model with a He-core mass of $4 M_{\odot}$ produces the best fit to the observed spectrum.

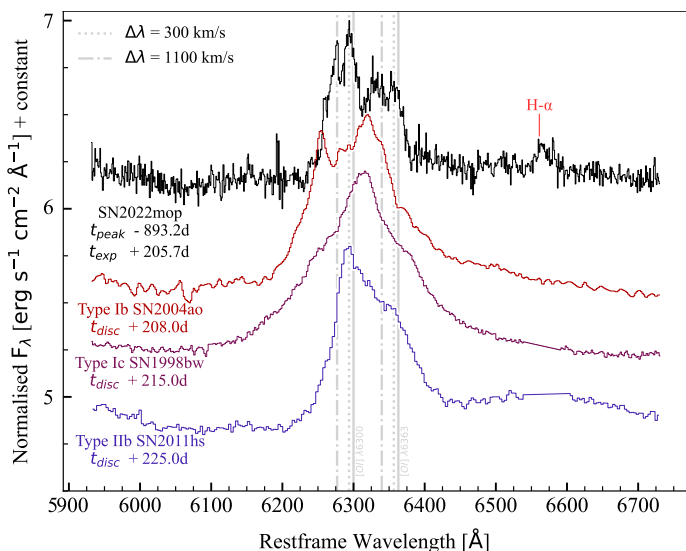


Fig. 9: Zoom-in of the [O I] $\lambda\lambda 6300, 6364$ profiles for SN 2022mop and other stripped-envelope SNe. In SN 2022mop, the [O I] emission is double-peaked, with the red and blue peaks offset by 300 km s^{-1} and 1100 km s^{-1} , respectively, from the rest wavelengths.

could argue otherwise, given the unique evolution of each transient – such as the late-time flaring in 2022 and the pre-supernova rise in mid-2024 – we are motivated to assume that both events occurred within the same binary system and interacted with each other.

4. Discussion

4.1. SN 2022mop and SN 2009ip-like transients

The eventful history of SN 2022mop is reminiscent of SN 2009ip (Pastorello et al. 2013; Fraser et al. 2015; Smith et al. 2020), as well as other interacting SNe that exhibit pre-SN activity (see Ofek et al. 2013; Strotjohann et al. 2021; Thöne et al. 2017; Elias-Rosa et al. 2016; Mauerhan et al. 2015; Fransson et al. 2022). In this area of transient research, pre-SN spectral observations are limited, with the only examples in the literature being SN 2009ip ($t_{\text{peak}} - 1122$ days; Smith et al. 2010; Foley et al. 2011; Pastorello et al. 2013), SN 2015bh ($t_{\text{peak}} - 558$ days; Thöne et al. 2017; Elias-Rosa et al. 2016), and SN 2023fyq ($t_{\text{peak}} - 103$ days; Brennan et al. 2024a). For these SNe, the chemical composition of the pre- and post-SN phases is consistent, and the spectral appearance is dominated by signs of ejecta or outflow colliding with the CSM. In the case of SN 2022mop, the nebular spectrum taken in 2022 is not consistent with the 2024 observations, suggesting two separate progenitors.

Using epochs with available *ugriz* bands, we construct a pseudo-bolometric light curve. These epochs include Lulin/SLT observations and span ± 10 days post-peak of the 2024 transient. We estimate the blackbody peak luminosity as $L_{\text{BB,peak}} \approx 7.8 \times 10^{42}$ erg, with an radiated energy over ± 10 days from peak of $L_{\text{int}} \approx 8.9 \times 10^{48}$ erg. This estimate is limited by low-cadence observations and sparse SED coverage but remains consistent with the Event B energetics of SN 2009ip ($\sim 10^{49}$ erg; Smith et al. 2014; Moriya 2015). Our first Lulin/SLT observations coincide with the initial rise of the 2024 event. During this period, the blackbody radius R_{BB} expands from $\approx 3.7 \times 10^{14}$ cm at -10 d to $\approx 1.1 \times 10^{15}$ cm at $+10$ d, while the blackbody temperature R_{BB} remains roughly constant at ~ 9000 K.

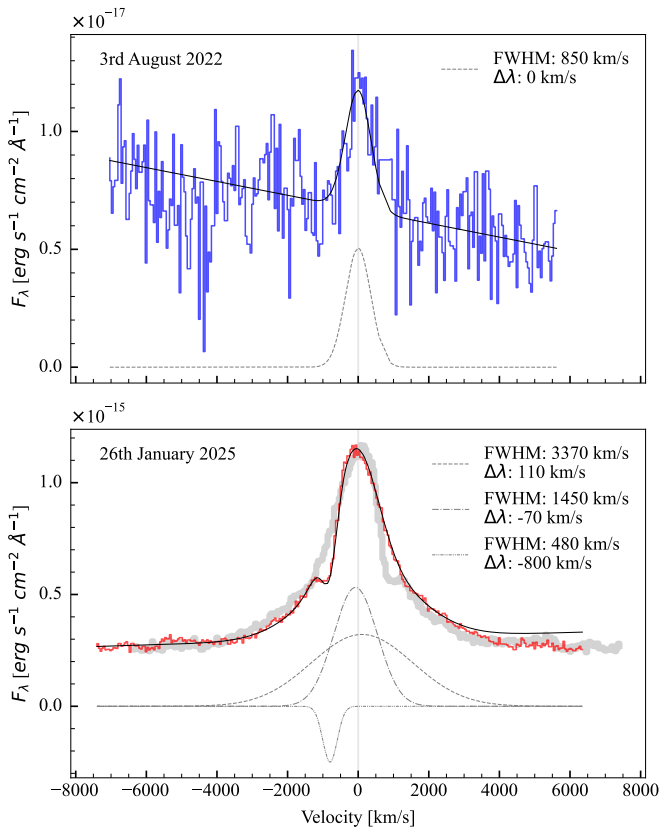


Fig. 10: Gaussian model fits to the $H\alpha$ profile on the 3rd August 2022 (top panel) and 26 January 2025 (bottom panel). The profiles are fitted using a flat continuum over the specified wavelength range. The $H\alpha$ profiles show a core FWHM of 850 and 1450 km s^{-1} respectively. Note that an unresolved (FWHM = ~ 135 km s^{-1}) noise spike at 6580\AA is removed from the 2022 spectrum. The post-peak spectrum shows broad emission with FWHM ≈ 3400 km s^{-1} and a P-Cygni-like feature with an absorption at -800 km s^{-1} . The thick grey band (lower panel) represents the reflected $H\alpha$ profile, highlighting the blueshifted $H\alpha$ emission with an extended red excess.

The collision of kinematically distinct material is an effective way to convert kinetic energy to radiation, and is typically the dominant power source for interacting SNe. Motivated by this, it has been suggested that several interacting SNe (e.g. Chugai et al. 2004; Dessart et al. 2009; Kochanek et al. 2012; Moriya 2015) may be non-terminal events, meaning the progenitor star has not undergone core collapse¹⁴. We consider the possibility that the 2024 transient is a result late time CSM interaction (e.g. SN 2014C and SN 2001em Margutti et al. 2017; Chandra et al. 2020).

Establishing that the two transients in SN 2022mop result from mass loss, core collapse, and *ejecta-shell* interaction is challenging, primarily due to the extreme brightness and energetics of the 2024 transient. The first episode

¹⁴ While these transients are commonly dubbed “SN Impostors” (Van Dyk et al. 2000; Van Dyk & Matheson 2012), we avoid the use of this nomenclature as it is clear that SN 2022mop underwent a genuine core collapse in 2022 due to the strong presence of [O I] $\lambda\lambda 6300, 6364$ (indicative of a large mass of oxygen), the emission from Co [II], and overall nebular appearance.

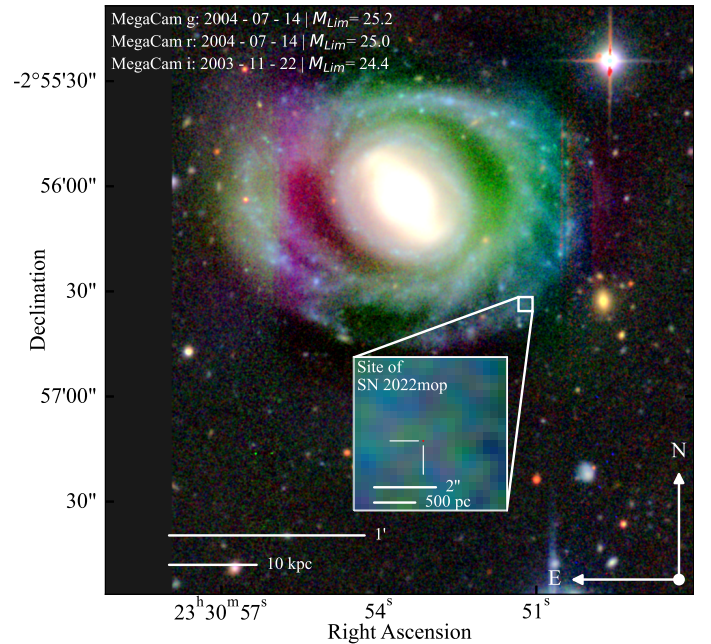


Fig. 11: CFHT/MegaCam *gri* composite image showing the lenticular host galaxy, IC 1496, and the location of SN 2022mop. No bright star-forming cluster is detected within the 1σ triangulation region, which, (for illustrative purposes) is indicated by the small red circle in the inset.

is followed approximately three years later by an even brighter transient (with energies akin to conventional CC-SNe; Taddia et al. 2013; Nyholm et al. 2020), which is difficult to explain outside the context of a pulsational pair-instability supernova (PPISN, which can effectively be ruled out from our August 2022 spectrum; Woosley 2017; Angus et al. 2024). Spectral modelling of the first transient suggests at least $1.6 M_{\odot}$ of ejecta. Assuming this material is travelling at ~ 3000 km s^{-1} (from our nebular modelling), it is expected to be at $\gtrsim 10^{16}$ cm, an order of magnitude greater than the blackbody radius at this time. This argument assumes that the blackbody radius captures the appropriate size of the 2024 event, which may be incorrect if asymmetries or clumping in the CSM is a factor.

Similar events have been observed, showing both spectral metamorphosis and rebrightening at late times (e.g., SNe 2001em and 2014C; Margutti et al. 2017; Chandra et al. 2020; Thomas et al. 2022). In previous examples, these rebrightening events were mainly observed in radio and X-ray wavelengths, whereas SN 2022mop exhibits strong optical emission. This difference in late-time evolution is likely an effect of the CSM optical depth. When the optical depth (τ) is greater than c/v (where v is the shock velocity), it primarily produces blackbody optical/UV emission, as observed for SN 2022mop. Conversely, when $\tau \ll c/v$, it powers bremsstrahlung X-ray emission as seen for SNe 2001em and 2014C (Margalit et al. 2022).

If the 2024 transient were influenced by the 2022 ejecta, the second transient should have occurred much earlier. The inconsistency in timing and energetics makes it difficult to reconcile the two events as being related to non-terminal mass-loss activity. Moreover, given that the second peak is brighter, it is reasonable to expect that the second event has greater kinetic energy, likely due to a larger ejecta mass or

higher velocity. This raises intriguing questions about how the progenitor system could generate two such energetic eruptions three years apart.

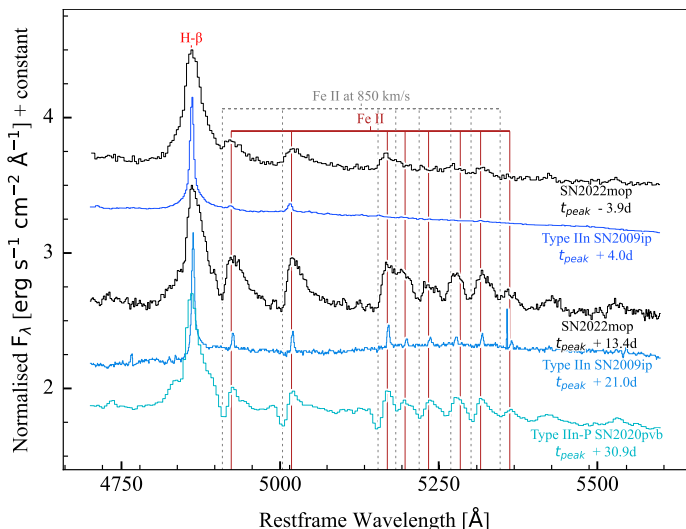


Fig. 12: The close-up of the approximate g -band wavelength range for several interacting transients. We highlight the unique Fe II emission lines that were not observed for SN 2009ip but are seen in several Type IIn SNe, e.g. SN 2020pvb (Elias-Rosa et al. 2024). The P Cygni emission for Fe II lines can be composed of a core emission profile with $\text{FWHM} = 2000 \text{ km s}^{-1}$ and an absorption profile at -850 km s^{-1} , similar to the $\text{H}\alpha$ profile given in Fig. 10.

A notable feature of the post-peak spectra of SN 2022mop is the strong Fe II emission, shown in Fig. 12. This emission resembles a P-Cygni-like profile with absorption at $\sim 800 \text{ km s}^{-1}$. Similar profiles have been observed in SNe 2011ht (Mauerhan & Smith 2012), 2020pvb (Elias-Rosa et al. 2024), 2016jbu (Kilpatrick et al. 2018; Brennan et al. 2022), and 2015bh (Elias-Rosa et al. 2016; Thöne et al. 2017). However, such profiles are not present in all SN 2009ip-like events, including SNe 2016bdu (Pastorello et al. 2018), and 2009ip itself.

4.2. A Hydrogen-Poor SN Followed by Mergerburst

We propose that the transients observed in 2022 and 2024 are physically related and originate from an interacting binary system, ultimately resulting in a “mergerburst” transient (Chevalier 2012; Soker & Kashi 2013; Pastorello et al. 2019)¹⁵. Mergerburst transients are driven by the in-spiral and coalescence of massive objects in binary systems with notable examples including V1309 Scorpii (Tylenda et al. 2011), and Eta Carinae (Portegies Zwart & van den Heuvel 2016; Smith 2013; Hirai et al. 2021).

Recent work by Tsuna et al. (2024a,b) has demonstrated that the precursor emission in SN 2009ip-like events, and the smooth rise observed in SN 2023fyq (Brennan et al. 2024b; Dong et al. 2024) can be explained by a progenitor star accreting onto a compact object (CO), culminating in a merger event (as suggested for SN 2009ip and similar transients by Soker & Kashi 2013; Kashi et al. 2013;

Soker & Gilkis 2018, and references therein). We demonstrate in Section. 3.1 that both the 2022 and 2024 events are coincident on the outskirts of IC 1496. In Section. 3.2, we model the nebular phase spectra and find our best fitting model, HE4P0, will result in a neutron star (NS) remnant, (see Figure. 3 in Ertl et al. 2020). Following the 2022 SN, the newly formed NS may acquire high proper motions due to sudden mass loss and natal kicks (Blaauw 1961; Giacobbo & Mapelli 2018; Hirai et al. 2024), with typical velocities of $100\text{--}300 \text{ km s}^{-1}$, occasionally exceeding 1000 km s^{-1} (Burrows et al. 2023). If the kick is sufficiently high ($\gtrsim 300 \text{ km s}^{-1}$) and directed appropriately, the NS may interact with its binary companion or its stellar wind/outflows (e.g., SN 2022jli; Moore et al. 2023; Chen 2024).

The NS may also receive post-natal slow acceleration that can accelerate it up to $\sim 1000 \text{ km s}^{-1}$ ($P_{\text{spin}}/1 \text{ ms})^{-2}$ (P_{spin} is the birth spin period of the NS) on timescales of months to years after the SN, by converting rotational energy into thrust (i.e. the Rocket mechanism; Harrison & Tademaru 1975; Hirai et al. 2024). For a tight mass-transferring binary system, the SN natal kick initially propels the system into a wider and more eccentric orbit. Achieving a direct merger through natal kicks alone is challenging, as it requires fine-tuned conditions within a narrow parameter space. However, once the system is in a wide orbit with a low orbital velocity, the relative influence of the rocket mechanism is enhanced (Hirai et al. 2024). If the rocket effect increases the eccentricity (e) sufficiently, approaching ~ 1 , it can induce a merger. This process occurs with a slightly higher probability, as it requires only two conditions: (a) the natal kick places the system into any sufficiently wide orbit (e.g. ~ 30 days from Fig. 4, sufficient to achieve $e \approx 1$; Hirai et al. 2024), and (b) the direction of the rocket-induced acceleration is somewhat aligned with the natal kick. The first condition is almost always satisfied due to the Blaauw kick (Blaauw 1961) and natal kick, while the second condition may also be relatively common if the suggested correlation between pulsar spin and kick alignment holds (e.g., Burrows et al. 2023).

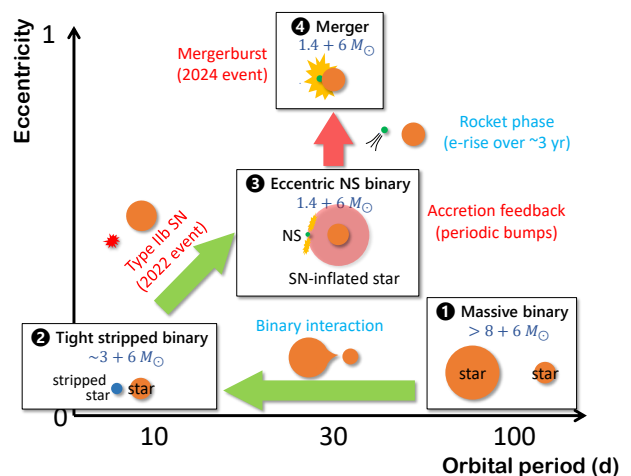


Fig. 13: Illustration of the proposed mergerburst scenario for SN 2022mop.

¹⁵ Or alternatively coined as a Merger-Precursor (Tsuna et al. 2024a,b).

As the newly formed NS follows an unstable eccentric orbit, it approaches the companion and previously ejected CSM material. Disruption of the outer layers may occur as the NS penetrates the outer envelope. As reported by Hirai & Podsiadlowski (2022), these NS-star envelope penetrations would likely be bound, and produce multiple collisions, on the timescales of \sim months, similar to that observed for SN 2009ip, and in 2022/2023 for SN 2022mop (see Fig. 2, these flaring events may also be due to periodic feedback from an accreting NS on an eccentric orbit). Due to drag forces within the common envelope, these interactions would subsequently decrease the collision velocity, effectively resulting in a decreased orbital period and cause an in-spiral¹⁶. This process transfers orbital energy to the envelope, possibly triggering eruption-like mass loss. The duration of these interactions depends on the initial orbit separation of the NS-star, as well as the magnitude of this drag forces (Hirai & Podsiadlowski 2022). An illustration of this scenario is given in Fig. 13.

For SN 2009ip, no SN-like (i.e. < -16 mag) event was observed since first observing the pre-SN progenitor (from HST/WFPC2 F606W in 1999; Foley et al. 2011), potentially meaning a much larger orbital separation or more eccentric initial orbit i.e. a longer time until complete merger.

The final outcome of NS-star interaction is unclear. The by-product of this scenario may be a luminous transient powered by super-Eddington accretion onto the engulfed NS (Chevalier 1996), which is likely to be radiatively inefficient and may power large outflows or jets (Moriya & Blinnikov 2021; Hirai & Podsiadlowski 2022; Soker 2022), possibly producing a ‘‘SN impostor’’ event, without disrupting the companion’s core. If the NS directly merges with the massive star’s core, the combined mass may exceed the *Tolman-Oppenheimer-Volkoff* mass (Oppenheimer & Volkoff 1939), i.e., the maximum mass of a non-rotating neutron star, triggering a violent collapse into a black hole (BH)¹⁷ or tidally disrupt the companion’s core entirely (Schröder et al. 2020), leading to a merger driven explosion. The formation of a BH may result in significant fallback of nucleosynthesised material, leading to a lack of an obvious nebular phase in SN 2009ip-like events, and potentially a large number of Type IIn SNe (e.g. Fox et al. 2013; Fraser et al. 2015; Benetti et al. 2016; Fox et al. 2020). Such significant fallback may also explain the relatively low-mass ejecta inferred for both Type IIn and Type IIn-p SNe, and also impact the mass of ejected ⁵⁶Ni.

Falsifying this explosion mechanism is difficult, as many of the suspected properties of such an explosion are akin to that of conventional Type IIn SNe (Moriya & Blinnikov 2021). Evidence may be found in late-time radio observations, where evidence of a binary induced merger may be collected (Dong et al. 2021; Thomas et al. 2022). Alterna-

tively the outcome may result in a transient arising from a common envelope ejection (CCE). This non-terminal explosion would likely leave behind a compact binary system (e.g. SN 2022jli; Moore et al. 2023; Chen et al. 2024a). This offers the potential for future deep observations to search for a surviving binary companion (e.g. SN 1993J; Maund et al. 2004; Fox et al. 2014).

5. Conclusions

We present a \sim 3-year observation campaign of SN 2022mop, a transient that initially exhibited nebular-phase emission in August 2022, resembling a Type Ib/IIB SN at +200 d, followed by a Type IIn event almost three years post-explosion in December 2024. We consider the possibility that the 2022 and 2024 events are isolated occurrences that coincidentally took place in the same region on the outskirts of their host galaxy. By triangulating the positions of both transients, we find that they are coincident to within a separation of \sim 3 pc. Given the low star formation rate in the immediate environment, and the peculiarity of both transients, we are motivated that both events originate from the same locality, likely representing a interacting binary system.

Using the SUMO radiative transfer code, we model the nebular emission and find a relatively unremarkable helium-rich progenitor, likely resulting in a NS remnant from a progenitor with $M_{ZAMS} \lesssim 18 M_{\odot}$. We postulate that this remnant enters an eccentric orbit, begins interacting with the companion star. The 2024 event resembles the *Event A/B* light curve seen in the SN 2009ip-like class of transients, with a rise time of \approx 4 months, reaching ~ -14 mag before transitioning into a Type IIn SN, which peaks at -18.2 mag.

SN 2022mop represents a compelling example where a compact object can be assumed to be bound to the system, making it a likely contributor to the production of the 2024 Type IIn transient via a merger-burst scenario, involving the newly formed NS and companion star. Continued insight into the possibility of this scenario can be achieved by identifying the pre-SN rise prior to the main SN event, and obtain high cadence photometry, searching for a decaying periodic orbit, a signature of an in-spiralling binary system. Additionally this scenario may emit gravitational waves (Renzo et al. 2021), which may be detectable with the next generation of space-based interferometers (e.g. Laser Interferometer Space Antenna (LISA); Amaro-Seoane et al. 2017) for very nearby transients. However more theoretical work, beyond the scope of this paper, is required to validate this claim.

Finally, we highlight the uniqueness of SN 2022mop. Without the 2022 Keck/LRIS spectrum presented in this work, SN 2022mop would be consistent with the general sample of SN 2009ip-like transients and potentially the overall population of interacting SNe. This unprecedented insight highlights the importance of considering binary interaction during the final stages of a massive star’s life. With the additional considerations presented in this work, we stress the necessity for future studies of late-time binary interaction in the context of pre-SN outbursts, SN 2009ip-like events, and the broader class of Type IIn SNe. This work is part of a two-part collection focusing on pre-SN variability, interacting SNe, and identification of such activity during the Rubin Era – see S. J. Brennan et

¹⁶ Traditionally, such encounters/collisions were assumed to result in an immediate merger, forming a Thorne–Żytkow object (TZO; Thorne & Żytkow 1975; Hirai & Podsiadlowski 2022) – a hypothetical system in which a NS core is embedded within a supergiant-like envelope.

¹⁷ This would be reminiscent of the *collapsar model* (Woosley & Heger 2006) (however, to date, no gamma-ray burst has been associated with an SN 2009ip-like transient, potentially due a result of a *choked-jet* scenario (Senno et al. 2016) due the progenitors extended envelope) or the core-merger-induced collapse (CMIC; Ablimit et al. 2022).

al. 2025, in prep. for continued discussion.

Acknowledgements. S. J. Brennan would like to thank David Jones for their help with the BLAST portal, as well as Takashi Moriya for their insights into merger models. SJB acknowledges their support by the European Research Council (ERC) under the European Union’s Horizon Europe research and innovation programme (grant agreement No. 10104229 - TransPIre). S. S is partially supported by LBNL Subcontract 7707915. SJS acknowledges funding from STFC Grants ST/Y001605/1, ST/X006506/1, ST/T000198/1, a Royal Society Research Professorship and the Hintze Charitable Foundation. AA and T.-W.C acknowledge the Yushan Young Fellow Program by the Ministry of Education, Taiwan for the financial support (MOE-111-YSFMS-0008-001-P1). This publication has made use of data collected at Lulin Observatory, partly supported by MoST grant 109-2112-M-008-001. N. S acknowledges support from the Knut and Alice Wallenberg Foundation through the “Gravity Meets Light” project and by and by the research environment grant “Gravitational Radiation and Electromagnetic Astrophysical Transients” (GREAT) funded by the Swedish Research Council (VR) under Dnr 2016-06012. W.J.-G. is supported by NASA through the NASA Hubble Fellowship grant HSTHF2-51558.001-A awarded by the Space Telescope Science Institute, which is operated by the Association of Universities for Research in Astronomy, Inc., for NASA, under contract NAS5-26555. A.J. acknowledges support by the European Research Council, the Swedish National Research Council, and the Knut and Alice Wallenberg foundation MN is supported by the European Research Council (ERC) under the European Union’s Horizon 2020 research and innovation programme (grant agreement No. 948381) and by UK Space Agency Grant No. ST/Y000692/1. A. S acknowledges their support from the Knut and Alice Wallenberg foundation through the “Gravity Meets Light” project. M.W.C acknowledges support from the National Science Foundation with grant numbers PHY-2308862 and PHY-2117997. Based on observations made with the Nordic Optical Telescope, owned in collaboration by the University of Turku and Aarhus University, and operated jointly by Aarhus University, the University of Turku, and the University of Oslo, representing Denmark, Finland, and Norway, the University of Iceland, and Stockholm University at the Observatorio del Roque de los Muchachos, La Palma, Spain, of the Instituto de Astrofísica de Canarias. Telescope time on this facility was made available under the Rubin LSST In-Kind program via the SWE-STK-S3 contribution. Pan-STARRS is a project of the Institute for Astronomy of the University of Hawaii, and is supported by the NASA SSO Near Earth Observation Program under grants 80NSSC18K0971, NNX14AM74G, NNX12AR65G, NNX13AQ47G, NNX08AR22G, 80NSSC21K1572, and by the State of Hawaii. Based on observations obtained with the Samuel Oschin 48-inch Telescope and the 60-inch Telescope at the Palomar Observatory as part of the Zwicky Transient Facility (ZTF) project. ZTF is supported by the National Science Foundation under Grant No. AST-2034437 and Award No. 2407588, as well as a collaboration including Caltech, IPAC, the Weizmann Institute of Science, the Oskar Klein Center at Stockholm University, the University of Maryland, Deutsches Elektronen-Synchrotron, Humboldt University, the TANGO Consortium of Taiwan, the University of Wisconsin at Milwaukee, Trinity College Dublin, Lawrence Livermore National Laboratories, IN2P3, the University of Warwick, Ruhr University Bochum, Cornell University, Northwestern University, Drexel University, the University of North Carolina at Chapel Hill, and the Institute of Science and Technology, Austria. Operations are conducted by Caltech’s Optical Observatory (COO), Caltech/IPAC, and the University of Washington at Seattle. The Gordon and Betty Moore Foundation, through both the Data-Driven Investigator Program and a dedicated grant, provided critical funding for SkyPortal. Funded by the European Union (ERC, project number 101042299, TransPIre). Views and opinions expressed are however those of the author(s) only and do not necessarily reflect those of the European Union or the European Research Council Executive Agency. Neither the European Union nor the granting authority can be held responsible for them.

References

Abazajian, K. N., Adelman-McCarthy, J. K., Agüeros, M. A., et al. 2009, *The Astrophysical Journal Supplement Series*, 182, 543
 Ablimit, I., Podsiadlowski, P., Hirai, R., & Wicker, J. 2022, *MNRAS*, 513, 4802

Amaro-Seoane, P., Audley, H., Babak, S., et al. 2017, arXiv e-prints, arXiv:1702.00786
 Angus, C. R., Woosley, S. E., Foley, R. J., et al. 2024, *ApJ*, 977, L41
 Astropy Collaboration, Price-Whelan, A. M., Lim, P. L., et al. 2022, *ApJ*, 935, 167
 Astropy Collaboration, Price-Whelan, A. M., Sipőcz, B. M., et al. 2018, *AJ*, 156, 123
 Astropy Collaboration, Robitaille, T. P., Tollerud, E. J., et al. 2013, *A&A*, 558, A33
 Barmtloot, S., Jerkstrand, A., Iwamoto, K., et al. 2024, *MNRAS*, 533, 1251
 Bazin, G., Palanque-Delabrouille, N., Rich, J., et al. 2009, *A&A*, 499, 653
 Bellm, E. C., Kulkarni, S. R., Graham, M. J., et al. 2019, *PASP*, 131, 018002
 Benetti, S., Chugai, N. N., Utrobin, V. P., et al. 2016, *MNRAS*, 456, 3296
 Blaauw, A. 1961, *Bull. Astron. Inst. Netherlands*, 15, 265
 Bradley, L., Sipőcz, B., Robitaille, T., et al. 2024, *astropy/photutils*: 2.0.2
 Brennan, S. J. & Fraser, M. 2022, *A&A*, 667, A62
 Brennan, S. J., Fraser, M., Johansson, J., et al. 2022, *MNRAS*, 513, 5642
 Brennan, S. J., Schulze, S., Lunnan, R., et al. 2024a, *A&A*, 690, A259
 Brennan, S. J., Sollerman, J., Irani, I., et al. 2024b, *A&A*, 684, L18
 Bufano, F., Pignata, G., Bersten, M., et al. 2014, *MNRAS*, 439, 1807
 Burrows, A., Wang, T., Vartanyan, D., & Coleman, M. S. B. 2023, arXiv e-prints, arXiv:2311.12109
 Cardelli, J. A., Clayton, G. C., & Mathis, J. S. 1989, *ApJ*, 345, 245
 Chambers, K. C., Boer, T. D., Bulger, J., et al. 2022, *Transient Name Server Discovery Report*, 2022-1650, 1
 Chambers, K. C., Magnier, E. A., Metcalfe, N., et al. 2016, arXiv e-prints, arXiv:1612.05560
 Chandra, P., Chevalier, R. A., Chugai, N., Milisavljevic, D., & Fransson, C. 2020, *ApJ*, 902, 55
 Chen, P. 2024, in *American Astronomical Society Meeting Abstracts*, Vol. 243, *American Astronomical Society Meeting Abstracts*, 349.04
 Chen, P., Gal-Yam, A., Sollerman, J., et al. 2024a, *Nature*, 625, 253
 Chen, T. W., Inserra, C., Fraser, M., et al. 2018, *ApJ*, 867, L31
 Chen, T.-W., Yang, S., Srivastav, S., et al. 2024b, arXiv e-prints, arXiv:2406.09270
 Chevalier, R. A. 1996, *ApJ*, 459, 322
 Chevalier, R. A. 2012, *ApJ*, 752, L2
 Chiosi, C. & Maeder, A. 1986, *ARA&A*, 24, 329
 Chugai, N. N., Blinnikov, S. I., Cumming, R. J., et al. 2004, *MNRAS*, 352, 1213
 Cochran, W. G. 1946, *The Annals of Mathematical Statistics*, 17, 164
 Cook, D. O., Kasliwal, M. M., Van Sistine, A., et al. 2019, *ApJ*, 880, 7
 Coughlin, M. W., Bloom, J. S., Nir, G., et al. 2023, *ApJS*, 267, 31
 Dahlén, T. & Fransson, C. 1999, *A&A*, 350, 349
 De, K., Kasliwal, M. M., Tzanidakis, A., et al. 2020, *ApJ*, 905, 58
 de Mink, S. E., Langer, N., Izzard, R. G., Sana, H., & de Koter, A. 2013, *ApJ*, 764, 166
 Dekany, R., Smith, R. M., Riddle, R., et al. 2020, *PASP*, 132, 038001
 Dessart, L., Hillier, D. J., Gezari, S., Basa, S., & Matheson, T. 2009, *MNRAS*, 394, 21
 Dessart, L., Hillier, D. J., Sukhbold, T., Woosley, S. E., & Janka, H. T. 2021, *A&A*, 656, A61
 Dessart, L., Hillier, D. J., Woosley, S. E., & Kunzarayakti, H. 2023, *A&A*, 677, A7
 Dong, D. Z., Hallinan, G., Nakar, E., et al. 2021, *Science*, 373, 1125
 Dong, Y., Tsuna, D., Valenti, S., et al. 2024, arXiv e-prints, arXiv:2405.04583
 Drake, A. J., Djorgovski, S. G., Mahabal, A., et al. 2009, *ApJ*, 696, 870
 Eldridge, J. J., Stanway, E. R., Xiao, L., et al. 2017, *PASA*, 34, e058
 Elia, D., Molinari, S., Schisano, E., et al. 2022, *ApJ*, 941, 162
 Elias-Rosa, N., Brennan, S. J., Benetti, S., et al. 2024, *A&A*, 686, A13
 Elias-Rosa, N., Pastorello, A., Benetti, S., et al. 2016, *MNRAS*, 463, 3894
 Ertl, T., Woosley, S. E., Sukhbold, T., & Janka, H. T. 2020, *ApJ*, 890, 51
 Foley, R. J., Berger, E., Fox, O., et al. 2011, *ApJ*, 732, 32
 Foreman-Mackey, D., Hogg, D. W., Lang, D., & Goodman, J. 2013, *PASP*, 125, 306
 Fox, O. D., Azalee Bostroem, K., Van Dyk, S. D., et al. 2014, *ApJ*, 790, 17

- Fox, O. D., Filippenko, A. V., Skrutskie, M. F., et al. 2013, *AJ*, 146, 2
- Fox, O. D., Fransson, C., Smith, N., et al. 2020, *MNRAS*, 498, 517
- Fransson, C., Sollerman, J., Strotjohann, N. L., et al. 2022, *A&A*, 666, A79
- Fraser, M., Kotak, R., Pastorello, A., et al. 2015, *MNRAS*, 453, 3886
- Fraser, M., Magee, M., Kotak, R., et al. 2013, *ApJ*, 779, L8
- Gal-Yam, A. 2017, in *Handbook of Supernovae*, ed. A. W. Alsabti & P. Murdin (Springer), 195
- Gal-Yam, A. 2021, in *American Astronomical Society Meeting Abstracts*, Vol. 237, American Astronomical Society Meeting Abstracts, 423.05
- Gal-Yam, A., Arcavi, I., Ofek, E. O., et al. 2014, *Nature*, 509, 471
- Gehrels, N., Chincarini, G., Giommi, P., et al. 2004, *ApJ*, 611, 1005
- Giacobbo, N. & Mapelli, M. 2018, *MNRAS*, 480, 2011
- Graham, M. J., Kulkarni, S. R., Bellm, E. C., et al. 2019, *PASP*, 131, 078001
- Harrison, E. R. & Tademaru, E. 1975, *ApJ*, 201, 447
- Hirai, R. & Podsiadlowski, P. 2022, *MNRAS*, 517, 4544
- Hirai, R., Podsiadlowski, P., Heger, A., & Nagakura, H. 2024, *ApJ*, 972, L18
- Hirai, R., Podsiadlowski, P., Owocki, S. P., Schneider, F. R. N., & Smith, N. 2021, *MNRAS*, 503, 4276
- Hu, L., Wang, L., Chen, X., & Yang, J. 2022, *ApJ*, 936, 157
- Jerkstrand, A. 2011, PhD thesis, Stockholm University
- Jerkstrand, A., Ergon, M., Smartt, S. J., et al. 2015, *A&A*, 573, A12
- Jerkstrand, A., Fransson, C., Maguire, K., et al. 2012, *A&A*, 546, A28
- Jerkstrand, A., Smartt, S. J., Fraser, M., et al. 2014, *MNRAS*, 439, 3694
- Jones, D. H., Read, M. A., Saunders, W., et al. 2009, *MNRAS*, 399, 683
- Jones, D. H., Saunders, W., Colless, M., et al. 2004, *MNRAS*, 355, 747
- Kashi, A., Soker, N., & Moskovitz, N. 2013, *MNRAS*, 436, 2484
- Kennicutt, Jr., R. C. 1998, *ARA&A*, 36, 189
- Kilpatrick, C. D., Foley, R. J., Drout, M. R., et al. 2018, *MNRAS*, 473, 4805
- Kochanek, C. S., Szczygiel, D. M., & Stanek, K. Z. 2012, *ApJ*, 758, 142
- Lang, D., Hogg, D. W., Mierle, K., Blanton, M., & Roweis, S. 2010, *AJ*, 139, 1782
- Laplace, E., Justham, S., Renzo, M., et al. 2021, *A&A*, 656, A58
- Leung, S.-C., Wu, S., & Fuller, J. 2021, *ApJ*, 923, 41
- Maeda, K., Kawabata, K., Mazzali, P. A., et al. 2008, *Science*, 319, 1220
- Magnier, E. A., Chambers, K. C., Flewelling, H. A., et al. 2020a, *ApJS*, 251, 3
- Magnier, E. A., Schlafly, E. F., Finkbeiner, D. P., et al. 2020b, *ApJS*, 251, 6
- Magnier, E. A., Sweeney, W. E., Chambers, K. C., et al. 2020c, *ApJS*, 251, 5
- Mainzer, A., Bauer, J., Cutri, R. M., et al. 2014, *ApJ*, 792, 30
- Marchant, P. & Bodensteiner, J. 2024, *ARA&A*, 62, 21
- Margalit, B., Quataert, E., & Ho, A. Y. Q. 2022, *ApJ*, 928, 122
- Margutti, R., Kamble, A., Milisavljevic, D., et al. 2017, *ApJ*, 835, 140
- Margutti, R., Milisavljevic, D., Soderberg, A. M., et al. 2014, *ApJ*, 780, 21
- Masci, F. 2013, arXiv e-prints, arXiv:1301.2718
- Masci, F. J., Laher, R. R., Rusholme, B., et al. 2019, *PASP*, 131, 018003
- Mauerhan, J. & Smith, N. 2012, *MNRAS*, 424, 2659
- Mauerhan, J. C., Van Dyk, S. D., Graham, M. L., et al. 2015, *MNRAS*, 447, 1922
- Maund, J. R., Smartt, S. J., Kudritzki, R. P., Podsiadlowski, P., & Gilmore, G. F. 2004, *Nature*, 427, 129
- McMillan, R. S., Larsen, J. A., Bressi, T. H., et al. 2015, *Proceedings of the International Astronomical Union*, 10, 317–318
- Meynet, G., Chomienne, V., Ekström, S., et al. 2015, *A&A*, 575, A60
- Modjaz, M., Blondin, S., Kirshner, R. P., et al. 2014, *AJ*, 147, 99
- Modjaz, M., Kirshner, R. P., Blondin, S., Challis, P., & Matheson, T. 2008, *The Astrophysical Journal*, 687, L9–L12
- Moore, T., Smartt, S. J., Nicholl, M., et al. 2023, *ApJ*, 956, L31
- Moriya, T. J. 2015, *ApJ*, 803, L26
- Moriya, T. J. & Blinnikov, S. I. 2021, *MNRAS*, 508, 74
- Newville, M., Otten, R., Nelson, A., et al. 2024, *lmfit/lmfit-py: 1.3.2*
- Niemela, V. S., Ruiz, M. T., & Phillips, M. M. 1985, *ApJ*, 289, 52
- Nyholm, A., Sollerman, J., Tartaglia, L., et al. 2020, *Å*, 637, A73
- Ofek, E. O., Sullivan, M., Cenko, S. B., et al. 2013, *Nature*, 494, 65
- Offner, S. S. R., Moe, M., Kratter, K. M., et al. 2023, in *Astronomical Society of the Pacific Conference Series*, Vol. 534, Protostars and Planets VII, ed. S. Inutsuka, Y. Aikawa, T. Muto, K. Tomida, & M. Tamura, 275
- Oke, J. B., Cohen, J. G., Carr, M., et al. 1995, *PASP*, 107, 375
- Oppenheimer, J. R. & Volkoff, G. M. 1939, *Phys. Rev.*, 55, 374
- Pastorello, A., Cappellaro, E., Inserra, C., et al. 2013, *ApJ*, 767, 1
- Pastorello, A., Kochanek, C. S., Fraser, M., et al. 2018, *MNRAS*, 474, 197
- Pastorello, A., Reguitti, A., Morales-Garoffolo, A., et al. 2019, *A&A*, 628, A93
- Patat, F., Cappellaro, E., Danziger, J., et al. 2001, *ApJ*, 555, 900
- Perley, D. A. 2019, *PASP*, 131, 084503
- Portegies Zwart, S. F. & van den Heuvel, E. P. J. 2016, *MNRAS*, 456, 3401
- Poznanski, D., Prochaska, J. X., & Bloom, J. S. 2012, *MNRAS*, 426, 1465
- Prentice, S. J., Ashall, C., James, P. A., et al. 2019, *MNRAS*, 485, 1559
- Prentice, S. J., Mazzali, P. A., Pian, E., et al. 2016, *MNRAS*, 458, 2973
- Prochaska, J. X., Hennawi, J., Cooke, R., et al. 2020a, pypeit/PypeIt: Release 1.0.0
- Prochaska, J. X., Hennawi, J. F., Westfall, K. B., et al. 2020b, arXiv e-prints, arXiv:2005.06505
- Prochaska, J. X., Hennawi, J. F., Westfall, K. B., et al. 2020, *Journal of Open Source Software*, 5, 2308
- Puls, J., Vink, J. S., & Najarro, F. 2008, *A&A Rev.*, 16, 209
- Ransome, C. L. & Villar, V. A. 2024, arXiv e-prints, arXiv:2409.10596
- Renzo, M., Callister, T., Chatziioannou, K., et al. 2021, *ApJ*, 919, 128
- Rodriguez, Ó., Maoz, D., & Nakar, E. 2023, *ApJ*, 955, 71
- Roming, P. W. A., Kennedy, T. E., Mason, K. O., et al. 2005, *Space Sci. Rev.*, 120, 95
- Rozwadowska, K., Vissani, F., & Cappellaro, E. 2021, *New A*, 83, 101498
- Salpeter, E. E. 1955, *ApJ*, 121, 161
- Sana, H., de Mink, S. E., de Koter, A., et al. 2012, *Science*, 337, 444
- Schlafly, E. F. & Finkbeiner, D. P. 2011, *ApJ*, 737, 103
- Schröder, S. L., MacLeod, M., Loeb, A., Vigna-Gómez, A., & Mandel, I. 2020, *ApJ*, 892, 13
- Senno, N., Murase, K., & Mészáros, P. 2016, *Physical Review D*, 93, 083001
- Shingles, L., Smith, K. W., Young, D. R., et al. 2021, *Transient Name Server AstroNote*, 7, 1
- Smartt, S. J. 2009, *ARA&A*, 47, 63
- Smith, K. W., Smartt, S. J., Young, D. R., et al. 2020, *PASP*, 132, 085002
- Smith, N. 2013, *MNRAS*, 429, 2366
- Smith, N. 2014, *ARA&A*, 52, 487
- Smith, N., Foley, R. J., & Filippenko, A. V. 2008, *ApJ*, 680, 568
- Smith, N., Mauerhan, J. C., & Prieto, J. L. 2014, *MNRAS*, 438, 1191
- Smith, N., Miller, A., Li, W., et al. 2010, *AJ*, 139, 1451
- Soderblom, D. R. 2010, *ARA&A*, 48, 581
- Soker, N. 2022, *MNRAS*, 516, 4942
- Soker, N. & Gilkis, A. 2018, *MNRAS*, 475, 1198
- Soker, N. & Kashi, A. 2013, *ApJ*, 764, L6
- Sollerman, J., Covarrubias, S., Chu, M., & Fremling, C. 2025, *Transient Name Server Classification Report*, 2025-54, 1
- Sollerman, J., Fransson, C., Barbarino, C., et al. 2020, *A&A*, 643, A79
- Spergel, D. N., Bean, R., Doré, O., et al. 2007, *ApJS*, 170, 377
- Srivastav, S., Stevance, H., Smartt, S. J., et al. 2025, *Transient Name Server AstroNote*, 2, 1
- Strotjohann, N. L., Ofek, E. O., Gal-Yam, A., et al. 2021, *ApJ*, 907, 99
- Taddia, F., Stritzinger, M. D., Bersten, M., et al. 2018, *A&A*, 609, A136
- Taddia, F., Stritzinger, M. D., Sollerman, J., et al. 2013, *A&A*, 555, A10
- Taubenberger, S., Valenti, S., Benetti, S., et al. 2009, *MNRAS*, 397, 677
- Thomas, B. P., Wheeler, J. C., Dwarkadas, V. V., et al. 2022, *ApJ*, 930, 57
- Thöne, C. C., de Ugarte Postigo, A., Leloudas, G., et al. 2017, *A&A*, 599, A129
- Thorne, K. S. & Zytkov, A. N. 1975, *ApJ*, 199, L19
- Tonry, J. L., Denneau, L., Flewelling, H., et al. 2018, *ApJ*, 867, 105
- Tsuna, D., Matsumoto, T., Wu, S. C., & Fuller, J. 2024a, *ApJ*, 966, 30
- Tsuna, D., Murase, K., & Moriya, T. J. 2023, *ApJ*, 952, 115
- Tsuna, D., Wu, S. C., Fuller, J., Dong, Y., & Piro, A. L. 2024b, *The Open Journal of Astrophysics*, 7, 82

- Tylenda, R., Hajduk, M., Kamiński, T., et al. 2011, *A&A*, 528, A114
- van Baal, B. F. A., Jerkstrand, A., Wongwathanarat, A., & Janka, H.-T. 2024, *MNRAS*, 532, 4106
- van der Walt, S., Crellin-Quick, A., & Bloom, J. 2019, *The Journal of Open Source Software*, 4, 1247
- Van Dyk, S. D. & Matheson, T. 2012, in *Astrophysics and Space Science Library*, Vol. 384, *Eta Carinae and the Supernova Impostors*, ed. K. Davidson & R. M. Humphreys, 249
- Van Dyk, S. D., Peng, C. Y., King, J. Y., et al. 2000, *PASP*, 112, 1532
- Vink, J. S. 2024, arXiv e-prints, arXiv:2406.16517
- Waters, C. Z., Magnier, E. A., Price, P. A., et al. 2020, *ApJS*, 251, 4
- Woosley, S. E. 2017, *ApJ*, 836, 244
- Woosley, S. E. 2019, *ApJ*, 878, 49
- Woosley, S. E. & Heger, A. 2006, *ApJ*, 637, 914
- Wright, E. L., Eisenhardt, P. R. M., Mainzer, A. K., et al. 2010, *AJ*, 140, 1868
- Yaron, O. & Gal-Yam, A. 2012, *PASP*, 124, 668
- Yaron, O., Perley, D. A., Gal-Yam, A., et al. 2017, *Nature Physics*, 13, 510
- Zapartas, E., de Mink, S. E., Izzard, R. G., et al. 2017, *A&A*, 601, A29

-
- ¹ The Oskar Klein Centre, Department of Astronomy, Stockholm University, AlbaNova, SE-10691 Stockholm, Sweden
- ² Center for Interdisciplinary Exploration and Research in Astrophysics, Northwestern University, 1800 Sherman Ave., Evanston, IL 60201, USA
- ³ Department of Physics, University of Oxford, Denys Wilkinson Building, Keble Road, Oxford OX1 3RH, UK
- ⁴ Astrophysics Research Centre, School of Mathematics and Physics, Queen's University Belfast, BT7 1NN, UK
- ⁵ Astrophysical Big Bang Laboratory, Cluster for Pioneering Research, RIKEN, Wako, Saitama 351-0198, Japan
- ⁶ School of Physics and Astronomy, Monash University, Clayton, VIC 3800, Australia
- ⁷ OzGrav: The ARC Centre of Excellence for Gravitational Wave Discovery, Clayton, VIC 3800, Australia
- ⁸ Department of Physics, University of Auckland, Private Bag 92019, Auckland, New Zealand
- ⁹ School of Physics, University College Dublin, L.M.I. Main Building, Beech Hill Road, Dublin 4 D04 P7W1, Ireland
- ¹⁰ Division of Physics, Mathematics and Astronomy, California Institute of Technology, Pasadena, CA 91125, USA
- ¹¹ Graduate Institute of Astronomy, National Central University, 300 Jhongda Road, 32001 Jhongli, Taiwan
- ¹² Caltech Optical Observatories, California Institute of Technology, 1200 E. California Blvd., Pasadena, CA 91125, USA
- ¹³ The Oskar Klein Centre, Department of Physics, Stockholm University, AlbaNova, SE-10691 Stockholm, Sweden
- ¹⁴ Astrophysics Research Centre, School of Mathematics and Physics, Queens University Belfast, Belfast BT7 1NN, UK
- ¹⁵ Instituto de Alta Investigación, Universidad de Tarapacá, Casilla 7D, Arica, Chile
- ¹⁶ Nordita, Stockholm University and KTH Royal Institute of Technology, Hannes Alfvéns väg 12, SE-106 91 Stockholm, Sweden
- ¹⁷ Institute for Astronomy, University of Hawaii, 2680 Woodlawn Drive, Honolulu HI 96822, USA
- ¹⁸ School of Physics and Astronomy, University of Minnesota, Minneapolis, Minnesota 55455, USA
- ¹⁹ Institute for Astronomy, University of Hawaii 34 Ohia Ku St., Makawao, HI 96768, USA
- ²⁰ IPAC, California Institute of Technology, 1200 E. California Blvd, Pasadena, CA 91125, USA
- ²¹ Space Telescope Science Institute, 3700 San Martin Drive, Baltimore, MD 21218, USA
- ²² Department of Physics and Astronomy, The Johns Hopkins University, 3400 North Charles Street, Baltimore, MD 21218, USA
- ²³ Institute for Astronomy, University of Hawaii, 34 Ohia Ku St., Pukalani, HI 96768-8288, USA

Appendix A: Observations logs and Reductions

A.1. Photometric Reductions

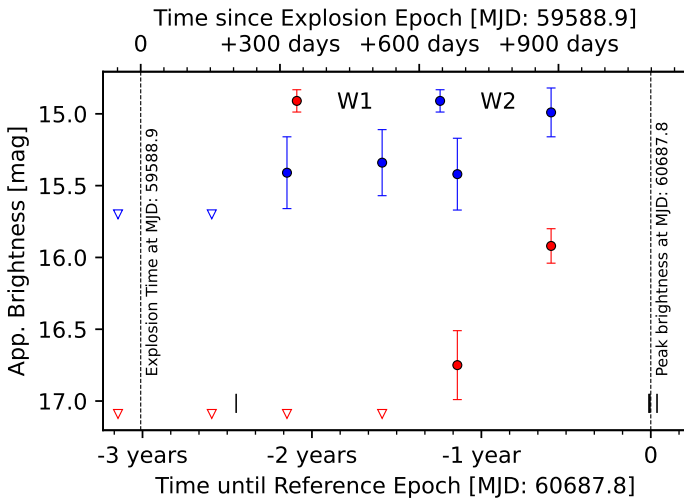


Fig. A.1: WISE Lightcurve of SN 2022mop with coverage extending before the 2022 transient of SN 2022mop as well as the initial rise before the 2024 event. While this may represent a late time rebrightening at longer wavelengths due to nebular emission from SN 2022mop, it is possible this reflects ongoing CSM interaction or dust formation.

The AutoPhOT pipeline (Brennan & Fraser 2022) was used to perform photometric measurements when a dedicated photometry service was unavailable, as well as to visually confirm pre-SN activity in the ZTF images. For each dataset, the target’s coordinates were obtained from the Transient Name Server (TNS; Gal-Yam 2021), and the World Coordinate System (WCS) values of the images were verified using *Astrometry.net* (Lang et al. 2010). An effective point spread function (ePSF) model was constructed using bright, isolated sources in the image with the *Photutils* package (Bradley et al. 2024). The PSF was fitted using a Markov Chain Monte Carlo (MCMC) approach, implemented in a custom MCMC fitter class within *LMFIT* (Newville et al. 2024) and *emcee* (Foreman-Mackey et al. 2013). This class defines the prior and likelihood functions based on the model parameters and incorporates the noise variance in the fitting procedure. The MCMC sampler was used to explore the parameter space and obtain the best-fit model parameters for position and flux, including uncertainties. The *griz* band zero-points were calibrated against sequence sources in the ATLAS All-Sky Stellar Reference Catalogue (REFCAT2; Tonry et al. 2018) and the Sloan Digital Sky Survey (SDSS; Abazajian et al. 2009) for *u*-band. Science and reference images were aligned using *Astropy*’s (*Astropy Collaboration et al. 2013, 2018, 2022*) *REPROJECT* function, and reference image subtraction was performed using the saccadic fast Fourier transform (SFFT) algorithm (Hu et al. 2022) to isolate any potential transient flux. If transient flux was not detected at a 5σ confidence level, the limiting magnitude of the image was determined via artificial source injection and recovery, as detailed in Brennan & Fraser (2022).

A.2. Spectroscopy

The complete spectroscopic dataset of SN 2022mop is presented in Fig. A.2 with an observational log given in Table. A.3. Calibrated spectra available on WISeREP (Yaron & Gal-Yam 2012).

Appendix B: Estimating the explosion time of SN 2022mop

We estimate the explosion time of SN 2022mop using the Bazin function (Bazin et al. 2009) based on flux measurements from the ATLAS forced photometry server. We estimate the explosion epoch (t_{exp}) as the peak (t_0) minus 3 times the rise time (t_{rise}) and report a value of $t_{\text{exp}} = 59589.9 \pm 5.5$ (around January 2022), see Fig. B.1. Given the low photometric cadence, this is a rough approximation to the explosion epoch.

Appendix C: SUMO setup

When preparing these models for SUMO, the ejecta are divided into seven different compositional zones. Named after their dominant elements, these are the Fe/He, Si/S, O/Si/S, O/Ne/Mg, O/C, He/C, and He/N zones. Of these zones, the first five are assumed to be fully macroscopically mixed, meaning that the zones are split into clumps of distinct composition. These clumps are then mixed in velocity space but retain their distinct composition (opposite to microscopic mixing, where all zones simply diffuse into a single “soup” of elements). We also mix in 40%, 18%, and 10% of the He/C zone into this core region for the $M_{\text{He, init}} = 3.3, 4.0,$ and $6.0 M_{\odot}$ models, respectively. This macroscopic mixing thus leads to the line widths and structures of most spectral lines in the nebular phase being very similar. From measurements of some of the lines in the SN 2022mop spectrum, we find that this macroscopically mixed core is contained within $V_{\text{core}} \sim 3000 \text{ km s}^{-1}$. We use this observation as a constraint in our spectral modelling by forcing the first five zones to be contained within 3000 km s^{-1} . Furthermore, we artificially increase the volume of the Fe/He and Si/S zones, as these zones are predicted to expand in the first few days after the SN due to radioactive heating, following the treatment described in Section 3.2.1 in Jerkstrand et al. (2015). Another change we make compared to the models by Woosley (2019) and Ertl et al. (2020) is the ^{56}Ni mass. The ^{56}Ni masses found in the original models ($\sim 0.02 - 0.04 M_{\odot}$) are significantly lower than what is found in observations, roughly $0.07 - 0.15 M_{\odot}$ (Prentice et al. 2016; Taddia et al. 2018; Prentice et al. 2019; Rodriguez et al. 2023). We therefore increase this mass by artificially increasing the mass of the Fe/He zone in the model, leaving its composition unchanged. The late-time lightcurve curve of SN 2022mop does not allow for an accurate ^{56}Ni estimate. Based on matching to the quasi-continuum flux in the observed spectrum, we set the ^{56}Ni mass in each model to $0.06 M_{\odot}$.

Appendix D: Triangulation of the 2024 transient

Data from Pan-STARRS provide images for both epochs, with a pixel scale of $0.258 \text{ arcsec/pixel}$, corresponding to a projected 88 parsec/pixel at the distance of IC 1496. We select epochs in September 2022 and October 2024 when the

Table A.1: Photometric log for SN 2022mop. The phase of each observation is given as $t_{\text{exp}} = 59588.9$ and $t_{\text{peak}} = 60687.8$. Full table available in online supplementary material.

Date	MJD	$t - t_{\text{peak}}$ (days)	$t - t_{\text{exp}}$ (days)	Magnitude	Error	Filter	ID
2022-01-13	59592.24	-1095.5	+3.3	18.832	0.144	o	ATLAS
2022-01-21	59600.23	-1087.5	+11.3	18.793	0.157	o	ATLAS
2022-06-02	59732.58	-955.2	+143.7	20.207	0.190	c	ATLAS
2022-06-06	59736.59	-951.2	+147.7	20.216	0.196	c	ATLAS
2022-06-10	59740.43	-947.4	+151.5	20.764	0.044	g	ZTF
2022-06-10	59740.46	-947.3	+151.6	20.610	0.031	r	ZTF
2022-06-11	59741.58	-946.2	+152.7	20.448	0.105	w	Pan-Starrs

Table A.2: Photometric log for SN 2022mop for WISE W1 and W2 bands. The phase of each observation is given as $t_{\text{exp}} = 59588.9$ and $t_{\text{peak}} = 60687.8$. We perform photometry on the subtracted images using a standard $8.25''$ radius aperture, applying suitable aperture corrections and zero magnitude fluxes for the WISE W1 and W2 bands (with central wavelengths of 3.4 and 4.6 μm , respectively) of $F_{\nu,0}^{W1} = 306.7$ Jy and $F_{\nu,0}^{W2} = 170.7$ Jy (Wright et al. 2010). Full table available in online supplementary material.

Date	MJD	$t - t_{\text{peak}}$ (days)	$t - t_{\text{exp}}$ (days)	μJy	$\Delta\mu\text{Jy}$	Magnitude	Error	Filter
2016-06-12	57551.00	-3136.8	-2037.9	>45.0	-	>17.09	-	W1
2016-06-12	57551.00	-3136.8	-2037.9	>90.0	-	>15.7	-	W2
2016-11-28	57720.00	-2967.8	-1868.9	>45.0	-	>17.09	-	W1
2016-11-28	57720.00	-2967.8	-1868.9	>90.0	-	>15.7	-	W2
2017-06-11	57915.00	-2772.8	-1673.9	>90.0	-	>15.7	-	W2

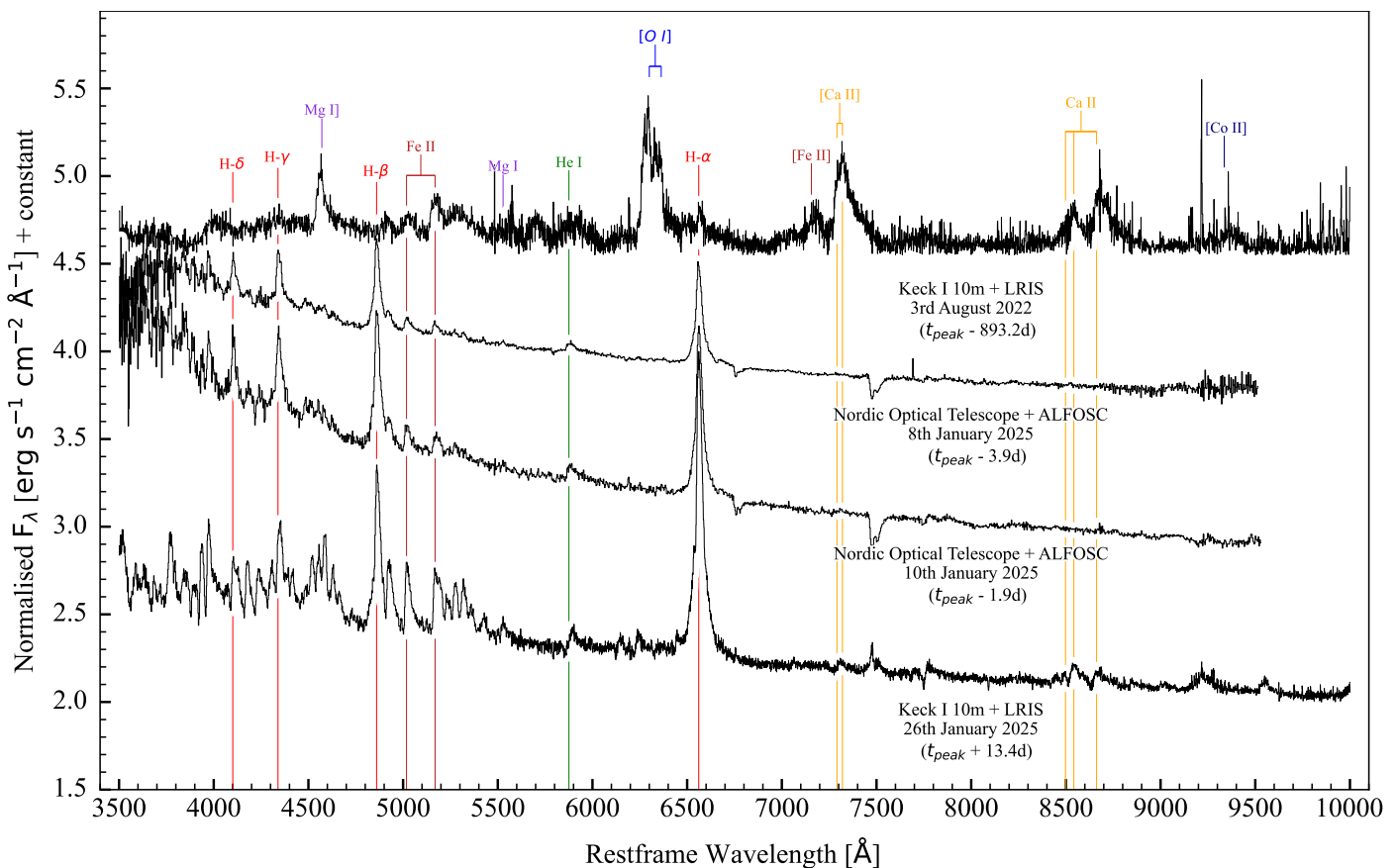


Fig. A.2: Spectroscopic observations for SN 2022mop. The phase of each observation is given as $t_{\text{peak}} = 60687.8$.

respective transients were at the approximate same magnitude. To triangulate the position of SN 2022mop, we build a set of 3-point asterisms using common sources in the 2022 image, employing two bright sources as anchor points,

and the position of SN 2022mop as the third vertex. An oversampled ePSF is constructed using the AutoPhOT code. Sources are excluded if their GAIA parallax exceeds 1 milli-arcsecond (which is smaller than the typical fitting errors

Table A.3: Spectroscopic log for SN 2022mop. The phase of each observation is given as $t_{\text{exp}} = 59588.9$ and $t_{\text{peak}} = 60687.8$. All spectra observed SN 2022mop using a $1''$ slit. Calibrated spectra available on WISeREP (Yaron & Gal-Yam 2012).

Date	MJD	$t - t_{\text{peak}}$ (days)	$t - t_{\text{exp}}$ (days)	Telescope	Instrument	Grating	Exposure (s)
2022-08-03	59794.6	-893.2	+205.7	Keck I 10m	LRIS	400/8500	900
2025-01-08	60683.9	-3.9	+1095.0	Nordic Optical Telescope	ALFOSC	Grism #4	1200
2025-01-10	60685.8	-1.9	+1096.9	Nordic Optical Telescope	ALFOSC	Grism #4	1200
2025-01-26	60701.2	+13.4	+1112.3	Keck I 10m	LRIS	400/8500	900

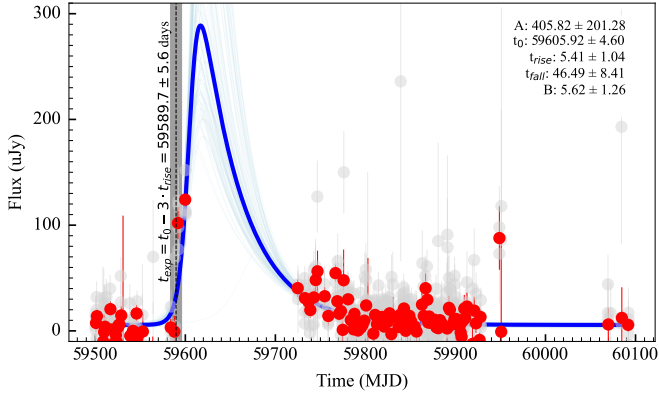


Fig. B.1: Estimate of the explosion time of SN 2022mop using a Bazin function fit. Grey points represent the raw data, while red points correspond to 1-day binned data. The blue lines show fits obtained using `emcee` sampling with the `LMFIT` package.

of each source), or if their PSF profile is extended (i.e., saturated, diffuse sources) in the either image. Using these pre-built asterisms, we project the expected 2022 position of SN 2022mop onto the 2024 Pan-STARRS images by using the same anchor sources and projecting the expected location on the third vertex. To account for position fitting error, we perform bootstrapped measurements by applying a pixel shift to each anchor position. These shifts follow a normal distribution with a standard deviation corresponding to the fitting error